# Calibration and Simulation of Astronomical X-ray Detectors


A thesis submitted towards partial fulfilment of
BS-MS Dual Degree Programme

by

Sujay Vivek Mate

Under the guidance of

Prof. Biswajit Paul

Raman Research Institute, Bangalore

Indian Institute of Science Education and Research Pune

# Certificate

This is to certify that this thesis entitled **Calibration and Simulation of Astronomical X-ray Detectors** submitted towards the partial fulfilment of the BS-MS dual degree programme at the Indian Institute of Science Education and Research Pune represents original research carried out by **Sujay Vivek Mate** at **Raman Research Institute**, under the supervision of **Prof. Biswajit Paul** during the academic year 2015-2016.

Sujay

Student
SUJAY MATE

Date : 22$^{nd}$ March 2016
Place : Pune

B. Paul

Supervisor
PROF. BISWAJIT PAUL

Date : 22$^{nd}$ March 2016
Place : Bangalore

# Declaration

I hereby declare that the matter embodied in the report entitled **Calibration and Simulation of Astronomical X-ray Detectors** are the results of the investigations carried out by me at the **Department of Astronomy and Astrophysics, Raman Research Institute**, under the supervision of **Prof. Biswajit Paul** and the same has not been submitted elsewhere for any other degree.

Student
SUJAY MATE

Date : 22$^{nd}$ March 2016
Place : Pune

Supervisor
PROF. BISWAJIT PAUL

Date : 22$^{nd}$ March 2016
Place : Bangalore

# Acknowledgements

I would like to thank Prof. Biswajit Paul, my supervisor, for giving me the opportunity to work on these projects and for his invaluable time and guidance without which this thesis work wouldn't have been possible. Working with him was a great experience and I have learned a lot during that period. I thank Mr. P.V. Rishin and Mr. M.R. Gopalakrishna of the X-ray lab, RRI, for giving me access to lab instruments and helping me set up and carry out experiments related to the X-ray polarimeter. Data acquisition from POLIX detector was carried under their supervision.

I would like to thank Dr. Santosh Vadawale of Physics Research Laboratory, Ahmedabad for his guidance in helping me understand Geant4. I am also thankful to Ms. Pragati Pradhan, graduate student, for her help in the work related to creation of response matrix for LAXPC. I also thank Dr. Chandreyee Maitra for sharing her work on response matrix. I am also grateful to RRI graduate students, Varun, Nazma, Gayathri, Raj, Karthik, Sourabh, Aru for their timely help. I would particularly like to thank Vidya ma'am, secretary of astronomy department, for her help in carrying out the required formalities and providing me with all the necessary facilities.

I would like to thank Dr. Prasad Subramanian for being a part of my Thesis Advisory Committee and for his valuable suggestions and help during the course of the thesis work.

Finally, I would like to thank my family and friends for their constant support over the last year.

# Abstract

To extract any astronomical information from the data obtained with a detector, detail knowledge of detector response and proper calibration is imperative. In this thesis, I present results obtained by carrying out calibration and simulations of two astronomical X-ray detectors. One of the instrument is *Large Area X-ray Proportional Counter (LAXPC)* which is a payload on recently launched Indian space observatory, ASTROSAT. The instrument is dedicated for timing and spectroscopic studies in energy range 3-80 keV. The second instrument is an X-ray polarimeter, POLIX, which is being developed at Raman Research Institute for a future satellite mission. The aim of this mission is to measure polarisation of X-ray sources in the energy range 5 - 50 keV.

In case of the proportional counters, the spectrum for incident radiation is measured in terms of the height of pulses produced by the individual X-ray photons. To interpret the data, the measured pulse heights must be converted into energy values. If we know the response of the detector for photons of various incident energies, we can transform the detector output from voltage values to energy values. The aim of the first part of my thesis work was to create this transformation matrix, called as response matrix. This was created by simulating detector response in Geant4 (a simulation toolkit for passage of particles through matter) for various energies. As the *LAXPC* consists of three detectors, the matrix was created for each one. The accuracy of matrix is checked by fitting it with well understood Crab spectrum obtained from the detector. Currently the matrix is fitting data very well in 6 - 30 keV range. However, outside this energy range, the observed spectrum and the measured spectrum shows some difference. Investigations are still in progress to address this problem.

Polarisation properties of astronomical sources in the high energy bands like X-ray and gamma ray are yet to be explored. As far as X-rays are concerned, many instrument developments are going on for measurements in energy range 2 - 8 keV using photo-electron track imaging, while in 30 - 200 keV band using Compton scattering method. The only experiment which works in intermediate band (5 to 30 keV) is a Thompson scattering X-ray polarimeter under development at Raman Research Institute, Bangalore for a future small satellite mission of the Indian Space Research Organization (ISRO). The detector geometry of the instrument is fixed with four square proportional counter detectors as four sides with a scatterer in the middle and a collimator on top. The aim of the second, important part of the thesis was to calibrate position determination from the ratio of the pulse height and to carry out simulations for given instrument configuration to optimise scatterer material, position and to find out modulation factor for the instrument. The simulations were carried out in Geant4. We report that best choice of scatterer material is Lithium-Beryllium combination kept at mid-way between centre and bottom of the detector. The modulation factor obtained for this configuration is 0.44. Also, Minimum Detectable Polarisation dependence on different intensities and different exposure time for Crab like sources for this modulation factor has been discussed.

# List of Figures

# List of Tables

# Contents

# Chapter 1

# Introduction

X-ray Astronomy is relatively new field than the conventional Optical Astronomy with a first detection of extra-solar X-ray source as late as 1962. Although, the existence of X-ray was established in late 19th century, any chance of ground based detection of astronomical X-rays sources was ruled out because of the opacity of atmosphere towards any high energy radiation. It took the dawn of the space age for astronomers to establish the existence of astronomical X-ray sources as the technology to send instruments high enough in the atmosphere became available. Since then a lot of missions (rockets/balloons/satellites) have flown to upper atmosphere/space and we have have discovered many X-ray sources and have learnt many things about physical processes at the root of such high energy emission.

My thesis is about instruments aboard two satellite missions for detection of X-rays, one current and one future. Last year (September 2015) Indian Space Research Organisation achieved another milestone by successfully launching maiden Indian Astronomy Satellite ASTROSAT. It is a multi-wavelength space observatory with detectors sensitive to wavelengths ranging from near ultraviolet to as high as hard X-rays ($\sim$150 keV). First part of my thesis consists of work related to one instrument, Large Area X-ray Proportional Counter (LAXPC), on board of ASTROSAT. As the name suggests, the instrument consists of proportional counters with large collecting area and is sensitive in energy range 3 to 80 keV. The aim here was to create response matrix for the instrument in this energy range. Second part of my thesis consists of calibration and simulations for future satellite mission, POLIX, dedicated for X-ray polarimetry. X-ray polarimetry is relatively unexplored field due to the difficulties in measuring the polarisation of X-rays. Raman Research Institute and ISRO are planning a small satellite mission for dedicated polarisation studies. The instrument, based on the principle of Thomson scattering, consists of a scatterer surrounded by four position sensitive proportional counters operating in 5 to 50 keV range . The aim of my work was to establish a calibration method for the detectors and carry out simulations to optimise the size, composition and position of the scatterer.

In this chapter, I will give a brief introduction to X-ray Astronomy (history, type of sources etc.). In the next chapter, I will explain the working of proportional counter detectors as they are at the heart of both the instruments. Chapter 3 describes the work related to LAXPC and Chapter 4 describes the work related to POLIX. Appendices include an introduction to software and algorithm used to carry out the simulations.

## 1.1 Introduction to X-ray Astronomy

Post World War II (1946 onwards), US Naval Research Laboratory was able to detect X-ray radiation from Sun by launching rockets into upper atmosphere, but the first cosmic source was observed by American Science and Engineering (AS&E) group led by Riccardo Giacconi on $18^{th}$ June 1962. The actual purpose of the experiment was to detect X-rays from Moon (produced by solar winds stopped by surface of the Moon) but instead they detected a strong flux of X-rays in the direction of constellation Scorpius and it was named as Sco X-1. This discovery gave astronomers better confidence in possibility of detecting X-ray sources. Over next decade many missions (rockets and balloons) were flown into the upper atmosphere in search of cosmic X-ray sources and most of them were great success. In 1970, Uhuru, the first satellite dedicated for X-ray detection was launched. The data from the satellite produced some outstanding results and a first X-ray all sky catalogue by scanning the entire sky was also created. After the success of Uhuru, many satellite missions have flown and have given us lot of insights about the X-ray universe. Currently many space observatories are operational in X-ray band but still we do not have complete understanding of X-ray sources and hence we can safely say that there is much more to explore about the X-ray universe.

Most of the X-ray point sources are binary systems with a compact object (Neutron star/ Black hole / White Dwarf) and a companion star. In such systems, the compact object accretes matter from the companion star and the falling matter forms a disk around the compact object. As the matter falls in, the gravitation potential energy is converted into heat which is emitted as radiation with a spectrum of blackbody. The peak of this spectrum falls in the X-ray band and hence most of the radiation from such system is dominated by X-rays. Another type of X-ray point source is Neutron star pulsar. Here the mechanism behind X-ray emission is believed to be combination of synchrotron, Compton scattering and blackbody. Similarly, distant Active Galactic Nuclei (AGN) are believed to be emitting X-rays by similar mechanisms. They are often accompanied by jets with diffuse X-ray emission coming out of the jets. Along with point sources, there are sources with diffuse emission as well. These are mostly galaxy clusters where intergalactic material falls towards the centre of the cluster emitting bremsstrahlung when high energy particles in such gas collide with each other. Along with these long lasting sources, there exits some transient X-ray sources (Supernovae/Gamma Ray Bursts) as well, where burst of energy is released when a high mass star is explodes. Most of the energy is released in the Gamma rays and X-rays. Exact mechanism for such emissions is still unknown. To summarize, there are many types of X-ray sources in the universe and we don't understand them completely even with half a century of study. To get better understanding we need to improve our detectors and their efficiency so that we can extract more information from incoming photons.

An astronomical observation can consist of one (or more) measurement(s) among four possible measurements, namely, Imaging (position), Photometry (timing and counts), Spectroscopy (energy), Polarimetry (polarisation of photons). A single detector can't measure all four quantities and we have to prioritise the quantities we are interested and build the detector accordingly. Also, in case of any detector, it is imperative that we know, as accurately as possible, how the

More details about history can be found in Reference [10]

detector behaves and what is its response towards various kind of radiation. To know this, one must carefully calibrate the instrument and record responses for various cases it may be subjected to in an actual observation. Hence, instrumentation is an important branch of Astronomy. As far as X-rays are concerned, building a efficient detectors is a not so trivial task as interaction of X-rays with matter has strong dependence on energy of the X-rays and the detector material. Hence, to detect X-rays, there are different types of detector for different energy ranges. Next chapter gives a brief review about various types of X-ray detectors in Astronomy and explains detailed working of one particular type, proportional counter, as both of the instruments which I have worked on are proportional counter detectors.

# Chapter 2

# Introduction to Proportional Counter Detectors

Major challenge in X-ray Astronomy is building efficient, affordable and robust detector with limitations on its size. All these requirements are due to the very fact that every detector is a payload for either a balloon, rocket or a satellite. Therefore, we have to plan dedicated mission for specific observables, compromising sensitivity in other observables. This translates into the fact that detector working principle and its sensitivity will depend on what kind of observations we want to do. I start this chapter with brief review of X-ray detector used in Astronomy [10] and then discuss one particular type of detector, namely, Proportional Counters, in detail [7].

## 2.1 Review of X-ray Detectors in Astronomy

Fundamental principle behind any X-ray detector is to collect energy deposition by the photo-electrons created from the interaction of X-rays with specific material volume inside the detector. The detector volume can be solid or gaseous depending upon what sensitivity and energy range one wants to achieve. Let us begin with most simple type of detector.

### 2.1.1 Proportional Counters

Proportional Counters are most simple and affordable X-ray detectors as they do not require special conditions, for example, low temperature, which is need for solid state detectors to work. Proportional Counters are special case of ionisation chamber detectors where the detector response is proportional to the ion-pairs created by the incident radiation. When an X-ray photon interacts within the active volume (usually a high Z inert gas), it creates photo-electrons. These electrons, when accelerated via high voltage, create many secondary electrons by process called avalanche. This charge is collected and it is amplified by electronics to produce a pulse. The amplitude of pulse is proportional to the photon energy, hence the name. The advantage of proportional counters is that two types of measurements can be easily done by them, namely, timing and counts (Photometry) and energy (Spectroscopy). Also, with a little modification, we can even do position sensitive measurements (Imaging) with limited accuracy.

Major drawback of such detectors is they are less efficient at energies above few tens of keV. This is because the detector volume is gas and at high energies photoelectric cross section drops significantly. Apart from that, because there is no control over avalanche, and the charge generated depends upon amount of avalanche, proportional counters don't have very good energy resolution. Also, large collecting area is required to detect fainter sources hence compromise on flux sensitivity has to be made when planning a mission based on size limitations of satellite. Moreover, in space, the leakage of gas through the X-ray window could be significant due to the high pressure difference; hence lifespan of such detectors is limited. Despite this, proportional counters are most used and reliable X-ray detectors and has been used on many of the X-ray missions.

### 2.1.2 Scintillation Counters

Scintillation Counters measure the secondary radiation (usually optical light emitted by ion-electron recombination) created by the incident X-rays. There are two types of scintillation counters, first type is where gas is used as active volume. Gas scintillation counters are similar to proportional counters except that instead of collecting the charge created by electron, optical fluorescence created by recombination is detected. They are better in energy resolution compared to proportional counters but not much efficient at high energies because of the gaseous active volume.

To increase efficiency at high energy more dense material is needed as an active volume. Second type of scintillation counters uses high density solid compounds with one element being a high Z element. The absorption of X-rays is much higher and they are efficient up to few MeV. In these detectors, amount of scintillation coming from crystal is detected. Scintillation counters are mostly used in balloon based missions.

### 2.1.3 Micro-Channel Plate

Micro-channel plate is a position sensitive detector which is used mostly for imaging. A Micro-channel plate consists of large number of small tubes (about few microns in diameter) called channel electron multiplier. High voltage is applied across the length of the tubes. Each tube is modified to emit large amount of secondary emission. When X-ray photon strikes the negative end it produces an electron, which is then accelerated through the potential across the length of the tube emitting large amount of secondary electrons. All these are collected at the end of the tube on a position sensitive plate. These are mostly used as imaging detectors. Some detectors on satellite missions such as Einstein, ROSAT and Chandra consists of Micro-Channel Plate.

### 2.1.4 Charge Coupled Devices

Charge Coupled Devices (CCDs) are most common radiation detectors used in optical, infrared and UV Astronomy. These can be effectively used for detecting low energy X-rays as well. CCDs are nothing but small photo-diodes attached together forming a matrix of *pixels*. When X-rays are incident on a pixel, they create electron-hole pairs, the number of which is

proportional to the X-ray energy. Since voltage is low there is no avalanche. The charge is readout row wise. Since charge is proportional to the energy and the position of interaction can be recorded by identifying pixel, CCDs can be used for Photometry, Imaging and Spectroscopy. Since the number of primary pairs is larger in CCDs and there is no secondary multiplication (which reduces uncertainty), energy resolution of CCDs is much better. Position resolution can be increased by shrinking the size of pixels. Only drawback back of CCDs is that they require focusing assembly (mirrors/lens for X-rays), which is difficult to build. Satellite such as Chandra, XMM-Newton, NuSTAR use CCDs with focusing optics to image X-ray sky in high resolution.

### 2.1.5 Calorimeter

Calorimeter is a revolutionary device with much better resolution than the energy resolution of CCDs. A Calorimeter consists of a crystal at very low temperature (30-50 mK). When an X-ray interacts with the crystal the temperature of the crystal changes due to the absorption of energy. This small change, which is proportional to the energy, is measured and the energy of the photon can be calculated. Major challenge in such detector is the keeping the temperature at such low value for a long time. First such detector was on Suzaku mission (2005) as one of the payload but unfortunately the refrigerator failed and hence data acquisition was not possible. Another instrument which uses this technique has flown on Astro-H mission on Feb. 17, 2016. As of now, the instrument is working fine and initial performance test are being carried out.

With brief information about various X-ray detectors, I will discuss about proportional counter in more detail as it is used in the instruments which I have worked on. In the next section I will introduce important concepts and properties of the proportional counters. Detail review of X-ray detectors can be found in Chapter 3 of Reference [10]

## 2.2 Operation and Properties of Proportional Counter Detectors

Proportional Counter detectors are special case of gas filled ionisation chamber detectors. Proportional counters were first introduced in 1940s. They are mostly used for detection of high energy radiation such as X-rays, but are also used for detection of particles such as alpha/beta particles or neutrons. In this section I will talk about the operation principle of proportional counters, important properties of proportional counters and one particular type of proportional counter, which is position sensitive proportional counter, since it is used in one of the instrument I worked on.

### 2.2.1 Principle of Operation

The process at the core of proportional counter detector operation is gas multiplication by avalanche formation. When a high energy radiation interacts with gas volume it creates multiple ion-electron pairs. If electric field is applied in this volume, the free electrons drift in the direction of electric field. At low values of field the electrons and ions simply drift towards

anode and cathode. But if the electric field is sufficiently high, the electrons can acquire additional energy and if this energy is more than ionisation energy of gas, these electrons can produce secondary ion-electron pairs. If the field is increased further, after certain threshold value, the secondary electrons are able to create more ion-electron pairs. Free electrons formed in this process can also create more ionisation and hence cascade is formed, named as Townsend avalanche. Townsend equation governs the fractional increase in the no. electrons per unit path length (Chapter 6 of Reference [7]),

$$\frac{dn}{n} = \alpha dx \tag{2–1}$$

Here $\alpha$ is first Townsend coefficient of the gas whose value is zero below certain threshold value of electric field but increase with the field above the threshold. Under proper conditions (appropriate voltage range, gas pressure and geometry), secondary ion-pairs can be kept proportional to the no. primary ion-pairs generated by the incident radiation. This is the region of proportionality and the gas multiplication is constant for given voltage in this region. Figure 2.1 show region of operation of proportional counters in comparison with other ionisation chamber detectors. Note that although the total charge collected varies exponentially with voltage, no. of secondary ion-pairs collected is always proportional to the primary ion-pairs.

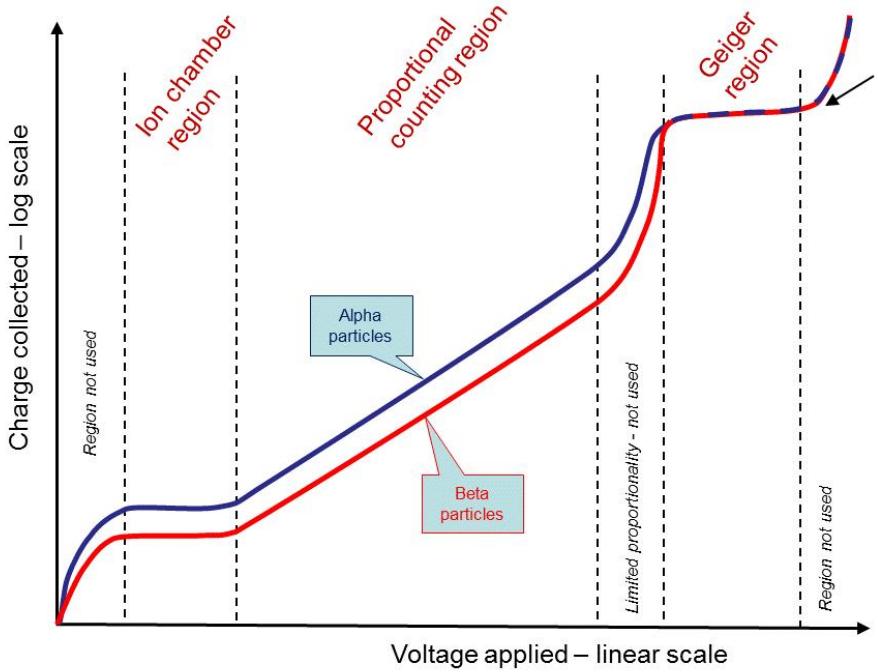


Figure 2.1: Region of operation of Proportional Counters. Image Source : Wikipedia

For constant field, $\alpha$ in equation 2–1 is constant and hence no. of electrons per unit length increases exponentially. In most proportional counters, cylindrical geometry is used. In such geometry an anode wire is placed at the axis of long hollow tube which serves as cathode. The tube is filled with the gas (see Fig 4.19b). In such geometry, the field increase rapidly close to the wire and hence no. electron created per unit path length are much more in contrast to the

constant field. Such geometry is preferred as large gas multiplication factor can be achieved even with relatively low values of voltage. The avalanche process in cylindrical detectors is depicted in fig. 2.3. Another advantage of cylindrical geometry is the avalanche is restricted to region very close to the anode wire where first interaction occurs. This fact can be used to determine the position of the event by making small modification to the output electronics (sec 2.3).

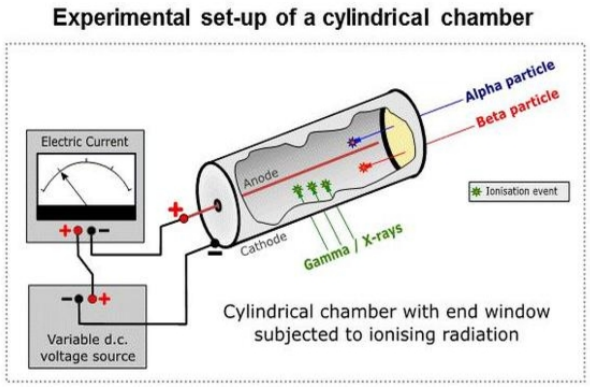


Figure 2.2: Schematic diagram of cylindrical geometry for proportional counter. Image Source : Wikipedia

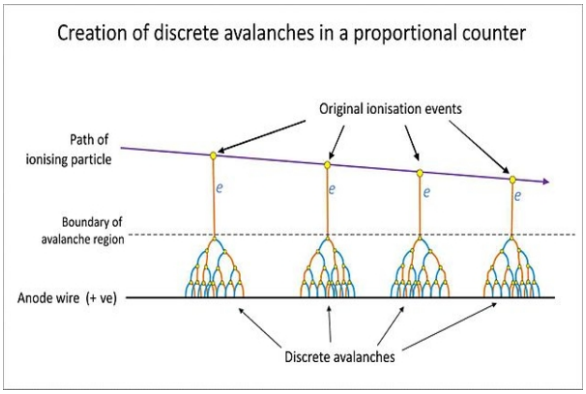


Figure 2.3: Avalanche process inside Proportional Counter (Scale is highly exaggerated). Image Source : Wikipedia

### 2.2.2 Mode of Operation and Pulse Amplitude Spectra

Mostly all the proportional counter detectors are operated in pulse mode. In such case, an output voltage pulse is generated when X-rays interact within the active volume and deposit charge on the anode wire. The amplitude of pule determines the total charge collected. Photons of similar energy would produce approximately similar amount of primary ion pairs. If the gas multiplication factor is constant, total charge produced will be proportional to the primary ion pairs. Hence pulse amplitude represents the energy of the incident photon. In all modern detectors, pulse amplitude is digitized and it is converted into a no. between 0 to $2^n - 1$ where $n$ is the no. of bits used in an Analog to Digital Converter.

While observing a source, the detector might be exposed to broadband energy source hence each event might produce different pulse amplitude. Even mono-energy source would produce slightly different amplitude because of statistical fluctuations. Hence it makes more sense to see pulse amplitude distribution (spectra) of source than to analyse individual pulse. Such a distribution has pulse amplitude (Channel No.) on x-axis and no. of pulses per channel on y-axis. It is also called *differential pulse height distribution*[1] because it represents no. pulses per channel between any channel C1 and C2. If we integrate the area under the curve we recover the total no. of pulses created which is nothing but the total no. incident photons. Therefore, pulse amplitude distribution represents energy spectra of incident source and hence it is an important property of a proportional counter.

### 2.2.3 Gas Multiplication Factor

Gas Multiplication Factor, usually denoted by $M$, is an important property of proportional counters. This is because total charge collected per event is given by,

$$Q = n_0 e M \tag{2–2}$$

where $n_0$ is no. of primary ion pairs generated by an event and $M$ is the gas multiplication factor. Since collected charge is of an utmost importance in operation of proportional counters, gas multiplication factor should not vary during operation. Gas multiplication mainly depends on gas used, anode voltage, radius of the anode cell, radius of the anode wire and the gas pressure. Dependence on anode voltage is most important since M varies exponentially with anode voltage[2]. Any small fluctuations in anode voltage can change M considerably, hence very stable voltage source should be used for proper operation.

### 2.2.4 Energy Resolution

As mentioned earlier, even mono-energy source produces different pulse amplitude because of the statistical fluctuations. These fluctuations arises because of the variation in no. of primary ion pairs and variation in gas multiplication factor. Due to this, pulse amplitude distribution for a mono-energy source has an intrinsic width. Total charge generated is given by the equation 2–2, hence the variance in Q is given by,

$$\left(\frac{\sigma_Q}{Q}\right)^2 = \left(\frac{\sigma_{n_0}}{n_0}\right)^2 + \left(\frac{\sigma_M}{M}\right)^2 \tag{2–3}$$

By empirical analysis and by assuming Polya probability distribution[3] for variation in gas multiplication factor, each term in right hand side of equation 2–3 is given by,

$$\left(\frac{\sigma_{n_0}}{n_0}\right)^2 = \frac{F}{n_0} \tag{2–4}$$

$$\left(\frac{\sigma_M}{M}\right)^2 = \frac{b}{n_0} \tag{2–5}$$

[1] Chapter 4 of Reference [7]
[2] Chapter 6 Section III A of Reference [7]
[3] Chapter 6 Section III C of Reference [7]

where F is fano factor for variance in no. of primary ion pairs generated and b is a constant due to the assumed probaility distribution. Hence the total variance in charge is given by,

$$\left(\frac{\sigma_Q}{Q}\right)^2 = \frac{F}{n_0} + \frac{b}{n_0} \tag{2–6}$$

Since $n_0$ is related to the energy of photon as $E = n_0 W$, where w is work function of gas, the variance in charge is related to the energy of incident photon as,

$$\frac{\sigma_Q}{Q} = \left(\frac{C}{E}\right)^{1/2} \quad where, C = W(F + b) \tag{2–7}$$

Since C is a constant for given gas, energy resolution goes as inverse of square root of photon energy. It also highly depends on the gas and hence any impurities inside the detector can affect the energy resolution. To achieve best resolution, usually noble gases are used as fill gas as they do not posses much of electron affinity and hence mobility of electrons is more inside the gas. Hence almost all the electrons created by avalanche are collected minimizing variation in gas multiplication.

## 2.3 Position Sensitive Proportional Counters

As mentioned earlier in sec 2.2.1, the overall avalanche process is limited to the portion of anode wire where first interaction occurs, hence we can determine the position of the interaction by small modification in the charge collection process. This type of proportional counter is of significance because the X-ray polarimeter which I worked on as part of this thesis (Chap. 4) uses position sensitive proportional counter.

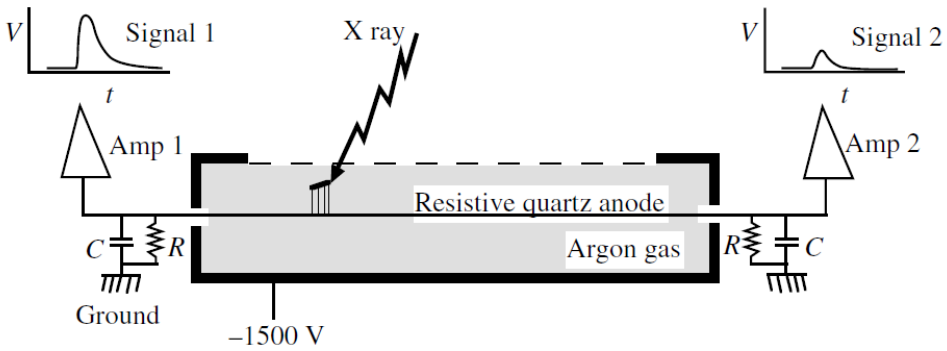


Figure 2.4: Schematic diagram of Position Sensitive Proportional Counter (In this case, by above eqn. the ratio value will be less than 0.5 as X-ray is interaction is close to Amp1). Figure adopted from Chapter 6 of Reference [3]

Basic principle used in position sensitive proportional counters is method of charge division. In this method, an anode wire with significant resistance per unit length is used and the charge is collected at the both ends of the wire (Fig. 2.4). Since the wire is resistive, the charge is divided into the ratio proportional to the ratio of resistance between two amplifiers and the position of interaction of the X-ray photon. By fixing one end as reference, we can get the

relative position as,

$$ratio = \frac{Amplitude\ at\ one\ end}{Total\ Amplitude} \tag{2–8}$$

This value is always fraction between 0 and 1. To get physical position, ratio values should be calibrated by selectively shinning X-rays at known physical positions. Since the resistance is linear, only two such measurements of ratio for known positions are sufficient to get the relation between relative position (ratio value) and physical position. One can use multiple wires, running parallel to each other but connected in series to get two dimensional localisation.

As I have introduced important properties of proportional counters, I stop the discussion about them at this point. Detail discussion about proportional counters as well many other radiation detectors can be found in Reference [7]. Next two chapters are about the work I carried out over past 8 months. Many of the concepts discussed here will be useful to understand the next two chapters.

# Chapter 3

# Creation of Response Matrix for LAXPC

Last year, Indian Space Research Organisation (ISRO) successfully launched maiden Indian astronomical observatory, *ASTROSAT*. The mission is joint efforts of 7 Indian and 2 foreign institutes with aim of doing multi-wavelength astronomical observations. Payloads on the satellite has energy range from UV to hard X-rays. One of the payload on the satellite is *Large Area X-ray Proportional Counter (LAXPC)*, dedicated for timing and spectroscopic studies, developed at *Tata Institute of Fundamental Research, Mumbai* with participation from *Raman Research Institute, Bangalore*. My work involved creation of response matrix for this detector by carrying out simulations in Geant4 [1]. This response matrix will be used to fit data recorded by the detector. I will first give a brief introduction about configuration of LAXPC and an introduction about response matrix before coming to the work carried out by me.

## 3.1 Introduction to LAXPC

As the name suggests, LAXPC is a proportional counter with large collecting area. LAXPC consists of 3 xenon gas proportional counter detectors, each with geometrical area of 3600 $cm^2$. The energy range is 2 to 80 keV. The total effective area of all the three detectors is greater than 6000 $cm^2$ for energy range 3-20 keV while it is above 2400 $cm^2$ for the entire energy band [9]. In this section I'll briefly discuss detector configuration and scientific goals LAXPC intend to achieve.

### 3.1.1 Configuration of LAXPC Detectors

Each LAXPC detector is a multi-wire proportional counter with dimensions of active volume as 100 × 36 × 15 cm. There are three extra layers of gas volume on two sides and one at the bottom as anti-coincidence volume. This layer is needed to discard cosmic ray events (discussed later in section). Dimensions of the layers which are on the two sides are 100 × 1.5 × 15 cm, while the one at the bottom has dimensions 100 × 39 × 1.5 cm. The active volume is divided into 5 vertical layers and 12 cells with an anode wire at the centre of each cell. Each cell hence has dimension 100 × 3 × 3 cm. Figure 3.1 shows the anode configuration of each detector.

Much of the discussion in this section follows Reference [8]

Wires in top two layers are connected alternatively forming 4 output anodes (A1, A2, A3, A4) within top two layers, while in remaining three layers all the wires are connected forming 3 output anodes (A5, A6, A7), one for each layer. Three anti-coincidence layer define three more output anodes (A8, A9, A10). Signal from each anode is collected and processed separately. The anti-coincidence anodes are used to discard false events created by cosmic ray interactions. As cosmic rays have high energy and are nearly isotropic in direction, they deposit energy in both, active and anti volumes and signal is seen in both anti anodes and detector anodes. Hence such events are discarded to avoid false detections. The gas volume is filled by 90% Xenon and 10% Methane. The pressure is about 2 atm, however exact value of pressure is slightly different for each detector. The detector top has a collimator with a Mylar layer between collimator and the detector volume.

The signal from each anode is amplified using Charge Sensitive Pre-Amplifiers (CSPA) which gives a voltage pulse. This pulse is digitised using a 10-bit ADC. Hence, pulse height distribution of each anode has total 1024 (0 to 1023) channels. However, the gain is set such that the 3-80 keV is covered by 24 to 640 ADC channels. A photon interaction inside a LAXPC detector can be of two type. One in which all the energy is deposited at one anode (single event) or second in which some energy is deposited at one anode and remaining at different anode (double event). Double events occur only when incident photon has energy greater than xenon K-edge (∼34 keV). In such case, if incident photon knocks out K-shell electron, a $K_\alpha$ (29.8 keV) or $K_\beta$ (33.64 keV) fluorescence is produced. The knocked out electron produces signal at the nearest anode while the fluorescence can either travel completely out of detector volume or might get absorbed at some other anode. In latter case, the double event is observed while is former case single event is observed. All the photons below K-edge produce single events only. Due to such interactions, the processed output of detector consists of two separate sets for each interaction. Each set contains information about anode number, pulse height amplitude (PHA) and a flag to indicate whether the event was a k-event or not (it is 1 if PHA lies between PHA values corresponding to Xe K-edge energies 25.5 - 34.5 keV). Because of such interactions and given anode configurations, it is possible to extract spectra in many different combinations. For example, one can do a selection on energy by only extracting those events where there are only single events and the the interaction occurs in top two layers (A1 to A4). As all low energy photons are absorbed in top layers, above selection is a selection on energy. To summarise, the configuration gives lot of flexibility in terms of spectral analysis.

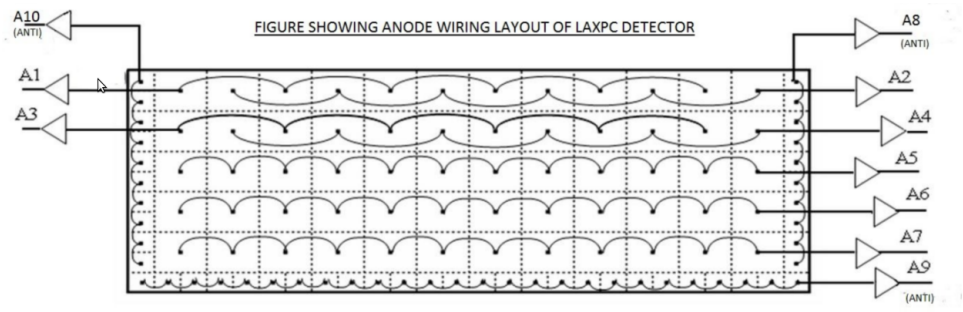


Figure 3.1: Cross-section of LAXPC detector along yz plane showing anode configuration. Image adopted from reference [8].

### 3.1.2 Major Scientific Goals of LAXPC

Due to its very good time resolution, LAXPC is perfect instrument to follow up transients discovered by X-ray monitors as well as observations of known persistent sources. As LAXPC has wide energy band with very high effective area over the entire energy band compared to any other instrument, it is perfect to observe and carry out broadband spectroscopic and timing studies of moderately bright and bright sources. This is aided by the fact that due to the near equatorial orbit of ASTROSAT, low and stable background rate is observed [9]. LAXPC, along with other instruments on ASTROSAT, aims to address following issues in greater detail,

- Broadband spectroscopy of X-ray sources
- Cyclotron Resonance Scattering Feature (CRSF) in accretion powered pulsars with high magnetic field
- Quasi Periodic Oscillations (QPOs) in the hard X-ray sources
- X-ray reprocessing and Thermonuclear bursts in accreting neutron stars
- Timing studies of Supergiant Fast X-ray Transients (SFXT)

As details about each issue is out of scope of this thesis, I have only listed them. More details about each issue and how LAXPC can help to address it can be found in Reference [9]. With this brief introduction about LAXPC, I will now discuss about what is a response matrix and why it so important factor in instrument development.

## 3.2 Response Matrix : Theory and Format

As it is clear from previous discussions, a proportional counter gives a spectra in terms of PHA channels. To make any physical interpretation, we need to convert this spectra in terms of energy. This can be done if we know what is the response of detector for every energy. As only discrete energy response can be recorded, the resulting distribution is called the response matrix. This section gives brief introduction about response matrix and how it is used to fit data and the standardised format in which it is mostly stored.

### 3.2.1 Mathematical Definition and Spectral Fitting

In an ideal case, response of a detector for a particular source is given as,

$$C(I) = \int_0^\infty f(E)R(I,E)dE \tag{3–1}$$

here $C(I)$ is observed counts for particular channel $I$, $f(E)$ is actual source spectrum in energy space and $R(I,E)$ is the instrument response which is defined as - the probability that incident photon of energy $E$ will be detected in channel $I$. Since we obtain instrument spectrum first we need to invert this relation to get the source spectrum. However, inversion of this relation is not

possible as it gives non-unique results and it is unstable w.r.t small changes in $C(I)$[1]. Better way is to go other way round. We can assume a source spectrum with some initial parameters. With this assumed spectrum and response $R(I, E)$ we can find the best fit to given data by varying the parameters.

In X-ray astronomy, most common software used for spectral fitting is *XSPEC*[2]. The software takes response file, data and spectral model as input and gives the best fit model with the final parameters. As it is not possible to create continuous response matrix the instrument team has to decide for what energy values the response matrix should be written. This mainly depends on the resolution of the detector in particular energy range and hence the energy values can be non-uniformly spaced. Ideally, the matrix should only have diagonal elements but due to finite energy resolution it contains off-diagonal elements as well.

### 3.2.2 Format of Response Matrix File

As *XSPEC* is a standard software used to analyse X-ray spectral data of any instrument, the format of response matrix must be standardised. The format is set by reference [4]. The response matrix is written in a FITS file with a .rmf (Redistribution Matrix File) extension. The file contains two extensions in form of binary tables along with null primary header. The two extensions are, EBOUNDS extension containing energy bounds for each channel and Redistribution Matrix Extension containing actual response matrix data. No. of rows in EBOUNDS extension depends on no. of detector channels, while no. of rows in MATRIX extension depends on no. energy values for which the response is written. In the matrix, rows represent energy while the columns represent channel no. The grid is filled with either zero or the probability of detection. To reduce the size, one can choose to write only those matrix elements where there is a non-zero value.

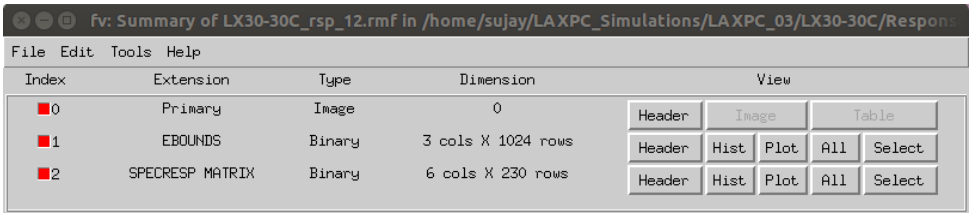


Figure 3.2: Format of .rmf file.

## 3.3 Generation of Response Matrix for LAXPC using Geant4

For LAXPC, the response matrix was created by carrying out simulations in Geant4[3] [1]. The entire process involved three stages. Calibration of detector using ground based calibration data to get the channel to energy conversion parameters; simulation of LAXPC detector in Geant4

[1] Section 3.1 of Reference [2]

[2] https://heasarc.gsfc.nasa.gov/xanadu/xspec/

[3] For more information about Geant4 see Appendix A

for set of energies and using above parameters to convert energy data from Geant4 to get simulated PHA distributions for each energy and writing the simulated PHA distribution data into RMF file. This process was carried out for all the three detectors. However, here I will only discuss results for LAXPC - 3 detector. Also, a pipeline for future run was set up by me as a part of the thesis work.

### 3.3.1 Calibration of LAXPC Detectors

Calibration of all three LAXPC detectors were done at TIFR using radioactive sources Am-241 (59.6 keV), Fe-55 (5.9 keV) and Cd-109 (22.16 keV, 21.9 keV, 24.91 keV and 88 keV) [8]. The calibration was done at three temperatures, 10℃, 20℃and 30℃. As there are no other mono-energy sources in the detector energy range, only these sources were used for calibration. I used the data from these calibration tests to get the channel to energy conversion parameters for each detectors. To get channel no. corresponding to these energies, background subtracted spectra for all the sources and for each anode was plotted and was fitted with a Gaussian. The mean value and sigma was noted for each energy and each anode. For Fe-55 source as the energy is too low, all the photons are absorbed in first layer (i.e. A1 and A2). There is no data in all the other anodes. The peak corresponds to 5.9 keV (Fig. 3.3). For Cd-109 source first two peak are not resolved by the detector and the detector shows combined main peak, however 3rd peak shows excess at higher end of the main peak (Fig. 3.4). Am-241 spectra is little more complicated. As the incident energy is 59.6 keV, which is more than Xe-edge, we see two escape peaks in the spectra along with a peak corresponding to 59.6 keV (Fig. 3.5). First escape peak (26 keV) is due to the $K_\beta$ fluorescence (33.6 keV) escaping the detector while second escape peak is due to the $K_\alpha$ fluorescence (29.8 keV) escaping the detector. Due to this we get additional calibration energies.

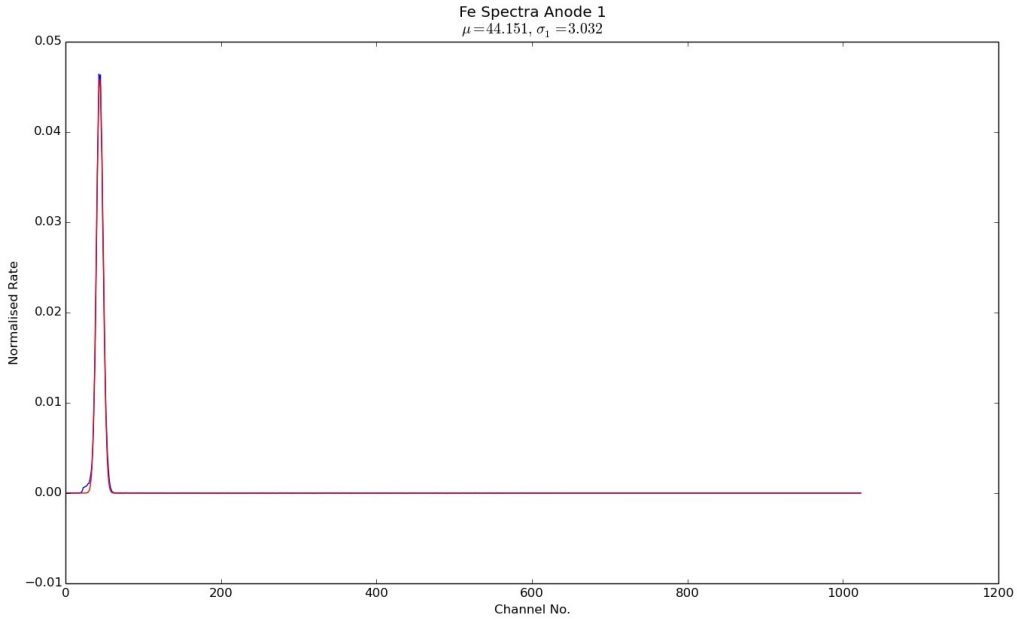


Figure 3.3: Fe spectrum for Anode 1 from LAXPC - 3 detector at 30℃

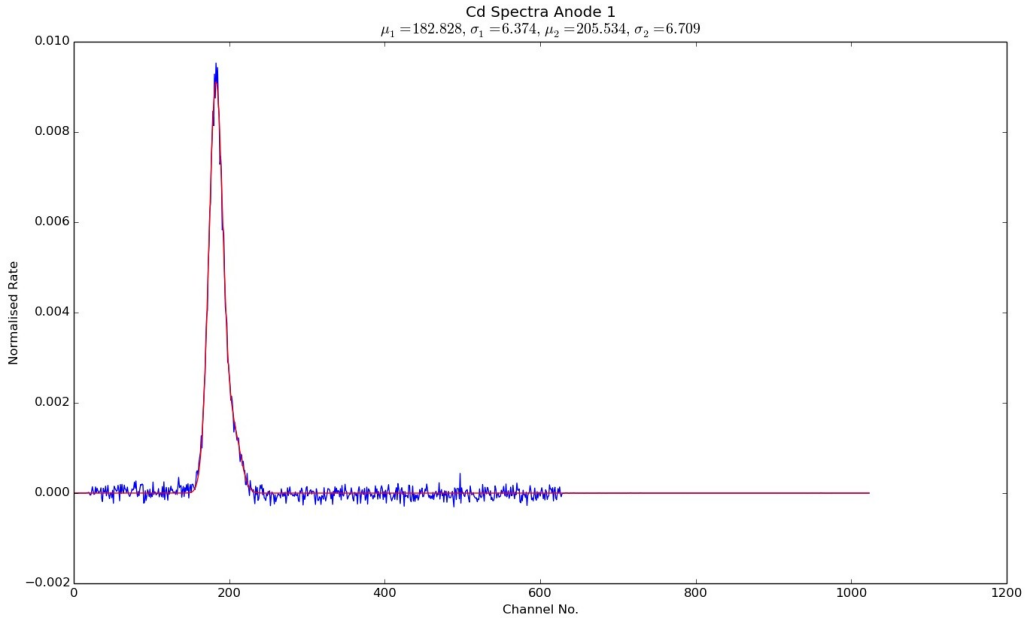


Figure 3.4: Cd spectrum for Anode 1 from LAXPC - 3 detector at 30°C

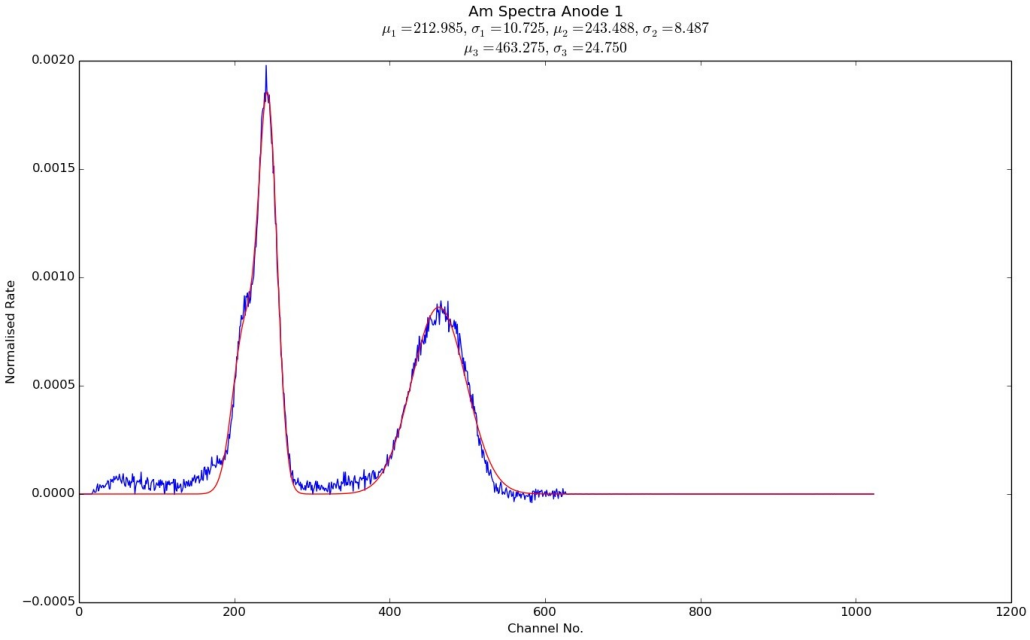


Figure 3.5: Am spectrum for Anode 1 from LAXPC - 3 detector at 30°C

As there are no other mono-energy sources, channel to energy correspondence for these energies was interpolated. Both mean value and sigma at each energy were interpolated using a quadratic fit. Quadratic fit was chosen as it was giving minimum variance compared to linear while cubic spline was giving non-physical values at lower energies. Fitting was done for each anode as gain for each anode varies slightly and hence the dependence is not uniform across anodes. To get one more data point at 5.9 keV for Anode 3 to 7, average of mean channel and sigma values for Anode 1 and 2 at same energy was used. The data was interpolated using following equation (both mean value and sigma values were interpolated using this relation),

$$chn/sigma = a + bE + cE^2 \tag{3–2}$$

where $E$ is energy in keV. Parameters $a, b, c$ were recorded for both mean channel values and sigma for each anode. These were written into files; separate for channel value and sigma values. Parameters for each anode were written row-wise in these files. These files were used to convert energy deposition information from Geant4 to channel numbers.

### 3.3.2 Simulation of LAXPC Detectors using Geant4

To create the response matrix, response of LAXPC detectors at various energies was simulated using Geant4. Actual geometry of LAXPC detector was created inside Geant with current pressure and gas mixture values. Photons were shined uniformly from the top and the interactions inside the detector were recorded in a file. The output was analysed using python scripts and using above energy to channel conversion parameters, the energy information was converted to detector channels to create simulated channel distribution . This distribution was then written into response matrix format discussed earlier by another external script. Here I will briefly discuss the Geant4 implementation and analysis algorithm used to get simulated channel distribution.

#### 3.3.2.1 Implementation in Geant4

To construct the LAXPC geometry, G4VUserDetectorConstruction class in Geant4 was used. As LAXPC is a simple detector with shape of a cuboid, inbuilt G4Box shape was used to create the active and anti volume and the Mylar window at the top. The volume was filled with 90% Xenon and 10% Methane. G4Material class was used to create the gas mixture. G4Material takes density, and mass fraction of mixture as input. Above composition translates to mass fraction 0.9866 for Xenon and 0.0134 for Methane. The density was calculated from the pressure (which is a known quantity for each detector) by assuming STP conditions.

Physical processes were simulated using predefined physics list G4EmLivermorePhysics. This physics list takes care of all the electromagnetic interactions. Atomic de-excitation was turned on to activate fluorescence and Auger electron emission. G4GeneralParticleSource was used to create incident photons. Photons were shined from above over all area using a planar source. The photon spectrum was mono-energy delta function. For initial tests, the simulation was carried out for 1 million photons, later the no. was reduced to 100000 photons. The final simulation was carried out for 230 energies in the energy range 2 to 120 keV (more than detector sensitivity range) with non uniform intervals. For lower energies since the resolution is low, interval between successive energies for which the simulation was carried out was as low as .1 keV while at very high energies it was increased to 1 keV.

Geant4 tracks all particle interactions inside the active volume. Using G4VUserSteppingAction class, all the locations and energy deposit at that location where photon (either source photon or fluorescence photon created inside active volume) is killed due to the photo electron creation were stored. The energy of the created photo electron was also assigned to the same location as such electrons have very small track length and it is absorbed at almost same location. This information was recorded for all the events which undergo interaction inside active or anti volume. For each energy, a file with above information for all the events was stored. This data

was analysed using python scripts which calculated total energy deposit and assigned anode numbers for each interactions.

#### 3.3.2.2 Analysis of Geant4 Output

The Geant4 output gives location in x, y, z co-ordinates and energy deposited at that location. To get spectrum for each anode, this information should be converted into energy deposited on each anode for each event first and then it should be converted to the detector channels. From this, one can create a simulated channel distribution. To perform these tasks, two python modules were written and they were called from a master python code to process Geant4 output file for each energy. The task of this first module was to assign an anode no. to each interaction information in the Geant4 output file, based on the co-ordinates. For a given event, the energy deposit information was added for a set of interactions where anode no. is same and the total energy is written against the anode number and the event number. To find the anode no. from co-ordinates, *scipy.spatial.KDTree* class was used. Methods in this class use K-D Tree algorithm to find the nearest neighbour of any point relative to a predefined point grid. As anode wires run in x-direction only two dimensional grid with yz co-ordinates was used. The grid points were anode wire y-z co-ordinates with centre of co-ordinate system coinciding with centre of yz cross section shown in Fig. 3.1. This module creates an output file where anode numbers and energy deposited in those anodes (two anode for each event in case of double event.) is for each event is written. If it is a single event zero is filled for at the place of second anode and energy deposition for second anode.

The second module converts this energy information to channel numbers using the conversion parameters obtained from interpretation of calibrated data. For each event in above file, parameters are selected based on anode number and equation 3–2 is used to convert energy to channel number and width. These values are then passed to *numpy.random.normal* function which returns a random number from the Gaussian distribution defined by channel number as mean and width as sigma. This creates the spread in energy which would be observed in the detector output because of the finite resolution. Before doing this, all the events which has detection in anti-layer are discarded as they are discarded in the detector as well. This module creates a spectra file similar to the LAXPC detector output file discussed in section 3.1.1 with anode no, PHA and k-flag as columns. The k-flag is set to one if PHA is between 200 to 280 channel number (same as detector logic).

From these files, channel distribution for each energy was extracted in a same way as spectra for detector is extracted. For single events PHA is assigned to the given anode. In case of double events, events in which there is one k-event, the PHA is summed and it is assigned to the anode whose k-flag is zero. While if both the events are k-events, PHA is summed and it is assigned to the anode which has minimum value among the two anodes. Double events with both k-flags as zero are discarded. Total channel distribution is then obtained by plotting histogram. One can obtain channel distribution for many combinations. Currently it is created for following combinations, distribution for each layer (total 5 ); distribution for the entire detector with all events (combined spectra for anode 1 to 7); distribution for the entire detector with only single

events and distribution for the entire detector with only double events. These combinations are created for each energy for which the simulations were carried out. From these distribution files, response matrix is created for each of these combinations (total 8 RMFs). While carrying out some initial tests we simulated spectrum for exact energies for which the calibration was done to check accuracy of the simulation. Figure 3.6 and 3.7 shows simulated and observed spectrum for anode 1 for Fe and Cd source.

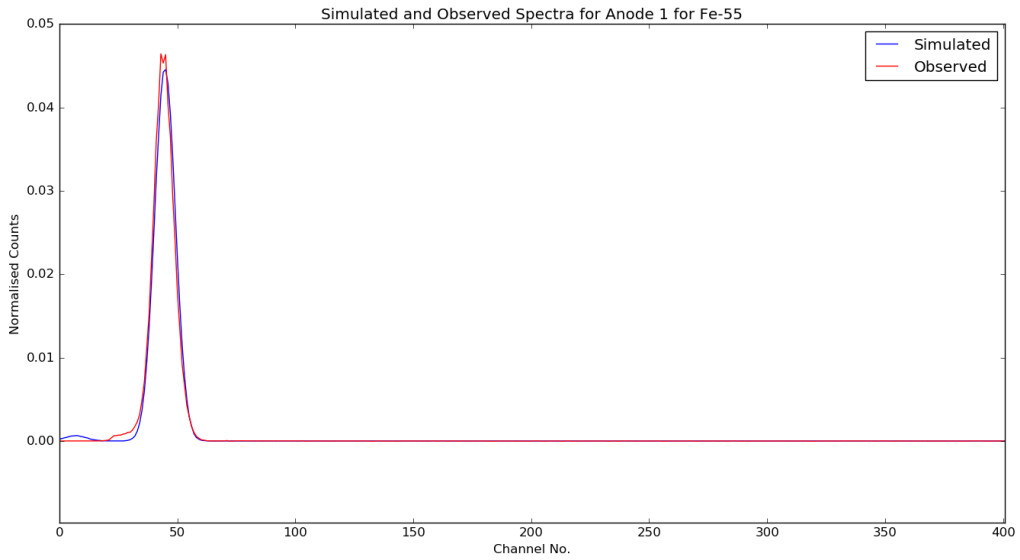


Figure 3.6: Simulated and observed spectrum for Anode 1 for Fe-55.

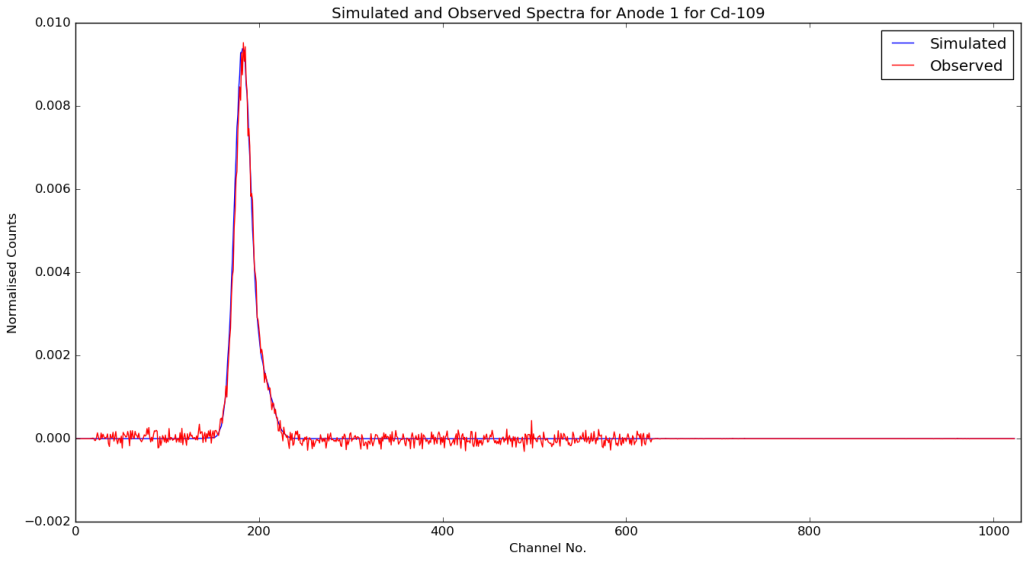


Figure 3.7: Simulated and observed spectrum for Anode 1 for Cd-109

### 3.3.3 Generation of Detector Response in Standard RMF Format

To store the channel distribution data in the standard RMF format discussed in section 3.2.2, a C program written by Dr. Chandreyee Maitra (RRI alumni) was used. The program was

modified according to current input parameters. To do this, first the user needs to create a rmf file using a standard template by running `ftemplate` command of `ftools`. This rmf file is then modified by the program and the matrix information is written to this file. The program takes following files as input,

- Two files storing energy bounds on channels for EBOUNDS extension.
- Two files storing bounds on simulated energy needed as columns inside MATRIX extension.
- File containing address of channel distribution files.
- Number of energies for which response is simulated.
- Name of the RMF file to which the response matrix is to be written.

As mentioned earlier, currently rmf files for all the 8 combinations mentioned in last section have been created. To check the accuracy of the response matrix it is fitted with the crab spectrum as crab is the most studied source and is a standard calibration. Results of which are discussed in next section.

## 3.4 Verification of Response Matrix Accuracy

To verify that the created response matrix is accurate enough, it was used to fit Crab spectrum observed by LAXPC. The spectral properties of Crab are well studied by many missions over the years and hence it is a standard calibration source for modern missions. Figure 3.8 shows observed Crab spectrum (LAXPC 3 detector) for entire detector (1 to 7 Anodes, black curve) and for different layers (coloured curves). The black curve is fitted with a power-law mode. The fit gives the photon index value of 1.95, while for Crab the value is 2.09. All the other

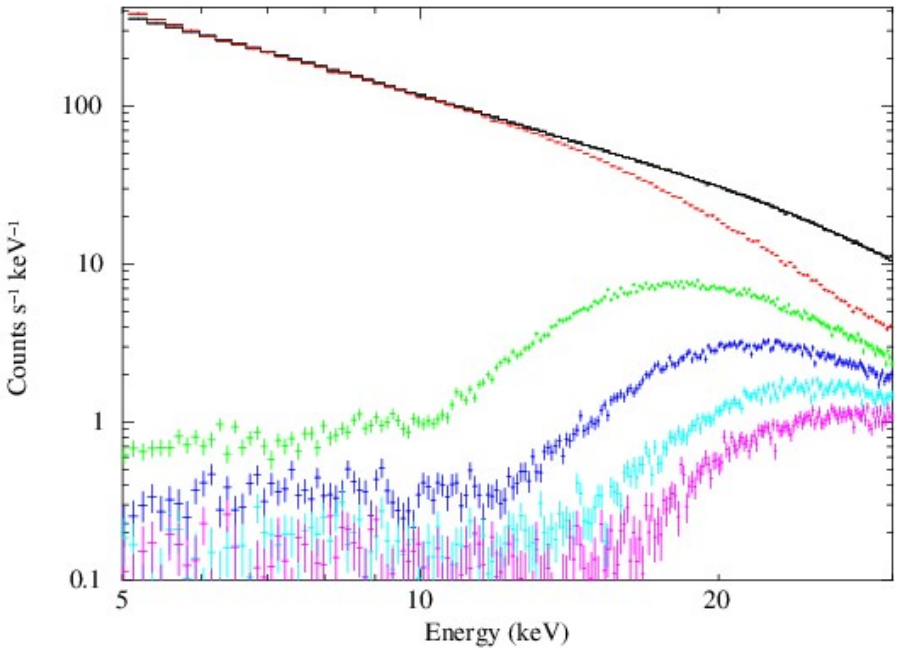


Figure 3.8: Crab spectrum fitted using response matrix. Plot created with XSPEC.

layers are yet to be fitted with layer-wise response matrix. Only 5 to 30 keV is shown because above 30 keV (after Xe-K edge to be precise) the fit generated using response matrix and the observed spectrum shows difference. Investigations are still in progress to address this problem. This might be due to the an error in handling double events in simulations or it might be a due to an error in handling double events in detector data. Both the fronts are being looked into for possible errors.

With this I conclude the discussion about creation of LAXPC. LAXPC and ASTROSAT mission in general shows great promise. We sincerely hope that it will give some exciting results in near future.

# Chapter 4

# Calibration and Simulations of X-ray Polarimeter

X-ray Polarimetry is relatively unexplored area and very few observations have been carried out and no dedicated X-ray polarisation has been flown in 40 years. With an excellent opportunity to carry out some pioneering work in this field, Raman Research Institute and Indian Space Research Organisation (ISRO) have planned a small satellite mission (POLIX) dedicated to X-ray polarisation measurements in low energy band (5-50 keV). Engineering model of the instrument is ready and the project has received a formal approval from ISRO for a launch about 3 years from now. Part of my thesis work was to establish a method to calibrate POLIX detectors and carry out simulations with the final detector geometry implemented to determine modulation factor and efficiency of the instrument.

## 4.1 Review of X-ray Polarimetry

Let us first begin with brief review about X-ray Polarimetry. In this section I will discuss about the need of polarisation measurements and will introduce some of the basic concepts related to polarisation measurements. Much of the discussion in this section is based on review paper cited as reference [6].

### 4.1.1 X-ray Polarisation Measurements : History and Necessity

Although X-ray astronomy has been an establish field for almost about 50 years and X-ray photometry, imaging and spectroscopy are very well developed, very few measurements have been done in the area of X-ray polarimetry. The only notable polarisation observation of X-rays had been recorded almost 40 years ago by OSO-8 mission [12]. The reason behind this is, to quote *Vadavale et. al.* [11], *"The main reason for the lack of X-ray polarisation measurements so far is their extremely photon hungry nature that severely limits the sensitivity"*. This means that polarisation measurements require a lot of exposure time to collect sufficient no. of photons but longer exposure implies higher background which affects the sensitivity. However, X-ray polarisation measurements are of significant importance as they can provide information about magnetic and gravitational field of compact X-ray sources such as neutron stars, AGN etc. This information is essential as it can be used to model such sources more accurately.

### 4.1.2 Polarisation Parameters for X-rays

If we shine a polarised light with angle of polarisation $\phi_0$ w.r.t. predefined x-axis on a rotating analyser, the light coming out of the analyser can be modelled by the modulation curve as,

$$S(\phi) = A + Bcos^2(\phi - \phi_0) \tag{4–1}$$

where $\phi$ is analyser angle w.r.t. the x-axis. The degree of polarisation (P) can be determined by the modulation amplitude as,

$$a = \frac{S_{max} - S_{min}}{S_{max} + S_{min}} = \frac{B}{2A + B} \tag{4–2}$$

This is true for ideal analysers but in real case, analysers do pass light even if the analyser angle is perpendicular to angle of polarisation. In such case, the degree of polarisation is determined by,

$$P = \frac{\mu}{\mu_{100}} \tag{4–3}$$

where $\mu$ is modulation amplitude/factor given by eqn. 4–2 for any sources and $\mu_{100}$ is modulation amplitude for source with 100% polarisation. In case of X-rays, $\mu_{100}$ is the property of instrument and it depends on the geometry and energy response of the instrument.

As mentioned earlier, measurement of polarisation in case of X-rays require large no. of photons. This requirement affects sensitivity as large amount of background is also collected. Hence, while measuring X-ray polarisation from a source it is important to quote a quantity which can state the accuracy with which the instrument can determine the polarisation. This quantity is called the 'Minimum Detectable Polarisation (MDP)'. The definition of this can be given as - MDP is the smallest polarisation value that can be measured with n-sigma confidence level. It depends on $\mu_{100}$, source count-rate, and background count-rate. The form is given by,

$$MDP = \frac{n_\sigma}{\mu_{100} S} \sqrt{\frac{S + B}{T}} \tag{4–4}$$

where,
S = Source count rate
B = Background count rate
T = Exposure time
$n_\sigma$ = Confidence level

From the eqn. it is clear that MDP is an instrument as well as source dependent quantity. With given instrument, for strong sources, we can determine small value of polarisation. But for weak sources even if polarisation value is high we might be limited by the MDP. Hence it is important to design the instrument to get reasonable value of MDP for broad range of source intensities. With this brief review about X-ray polarimetry and some important concepts I bring this discussion to the halt. I will now proceed to briefly introduce the design and operation principle of POLIX.

## 4.2 Introduction to POLIX

POLIX is based on standard method of Thomson Scattering to measure the polarisation of X-rays. Although more precise method such as photo-electron track imaging have been developed, it requires much large scale mission. Hence Thomson Scattering method is used which fits in the scale of the mission [11]. Let us first discuss the principle on which the polarimeter is based on.

### 4.2.1 Principle of Detection : Thomson Scattering Method

Schematic diagram of Thomson scattering method for polarisation measurement is given in Fig. 4.1. Differential Thomson scattering cross section for polarised light is given by,

$$\frac{d\sigma}{d\Omega} = r_e^2 sin^2\Theta \tag{4–5}$$

where, $r_e^2$ is classical electron radius and $\Theta$ is angle between direction of electric field of incident radiation and direction of scattered radiation. This can be converted to angles defined in Fig. 4.1 where, $\theta$ is usual polar angle and $\phi$ is the azimuthal angle. Then the cross section takes the form [11],

$$d\sigma = r_e^2(1 - sin^2\theta cos^2\phi)d\theta d\phi \tag{4–6}$$

By measuring the angular distribution of scattered photon we can determine the polarisation of incident photons. The angular distribution is measured by plotting the modulation curve discussed in Sec. 4.1.2. In short, the scatterer acts as an analyser and by placing detector around the scatterer we can observe the modulation curve (equivalent to rotation of analyser). In such case, the modulation pattern is given by [11],

$$C(\phi) = Acos(2(\phi - \eta + \frac{\pi}{2})) + B \tag{4–7}$$

where, $\phi$ is azimuthal angle and $\eta$ is angle of polarisation. Notice that the modulation is symmetric under rotation by 180 degrees similar to the angle of polarisation. The modulation factor is defined as in eqn. 4–2. Only in this case, $\mu$ in terms of $A$ and $B$ is given by,

$$\mu = \frac{A}{B} \tag{4–8}$$

The degree of polarisation is same as defined by the eqn. 4–3. To measure angular distribution, position sensitive proportional counters can be used as detector surrounding the scatterer. The major disadvantage of this method is that the large fraction of photons are lost because of the forward or back scattering of photons. Hence to achieve reasonable MDP, long exposure is needed. In the next section I will describe the geometry and instrument details of POLIX.

### 4.2.2 POLIX Instrument Design

The current design for X-ray polarimeter, POLIX, is shown in Figure 4.2. This is final engineering model and only small changes might be done depending on the space verification test and vibration test results. The instrument consists of a scatterer in middle surrounded

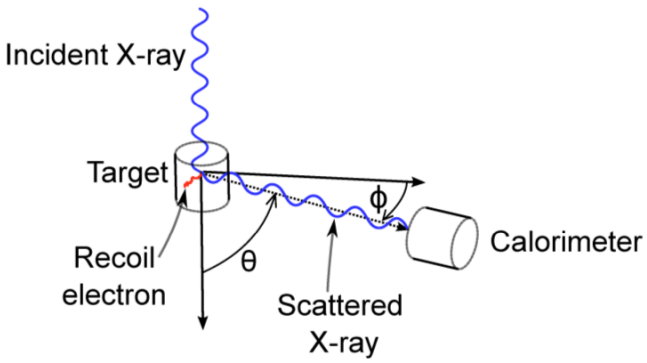


Figure 4.1: Schematic Diagram for Thomson scattering Polarimeter. Here, Calorimeter can be replaced by more simpler detectors such as proportional counters. Figure adopted from Reference [6]

by four square position sensitive proportional counters. A collimator on top is used to restrict the field of view. Each position sensitive proportional counter contains 12 anode wires running vertically, i.e. perpendicular to the scatterer plane. Out of 12 wires first 6 wires are connected in series by connecting alternate top an bottom end serving as one single wire and giving 2-D spatial resolution as position on six wires can be determine by method described in Sec. 2.3. Remaining 6 wires form another such set. Data from each set is collected separately forming two output channels (not to be confused with channel no. in pulse height spectra sec 2.2.2) per detector. Each proportional counter volume have an offset w.r.t. the centre of the instrument (i.e centre of scatterer.) due to the reason related to structural stability. Figure 4.3 shows the detector offset. Image is directly saved from visualisation created by Geant4 toolkit used for simulations discussed in Sec. 4.4. Depth of proportional counter volume is about 4.5 cm. Xenon gas is used as fill gas and the pressure will be about 800 torr. The instrument will be designed to rotate as shown in Figure 4.2.

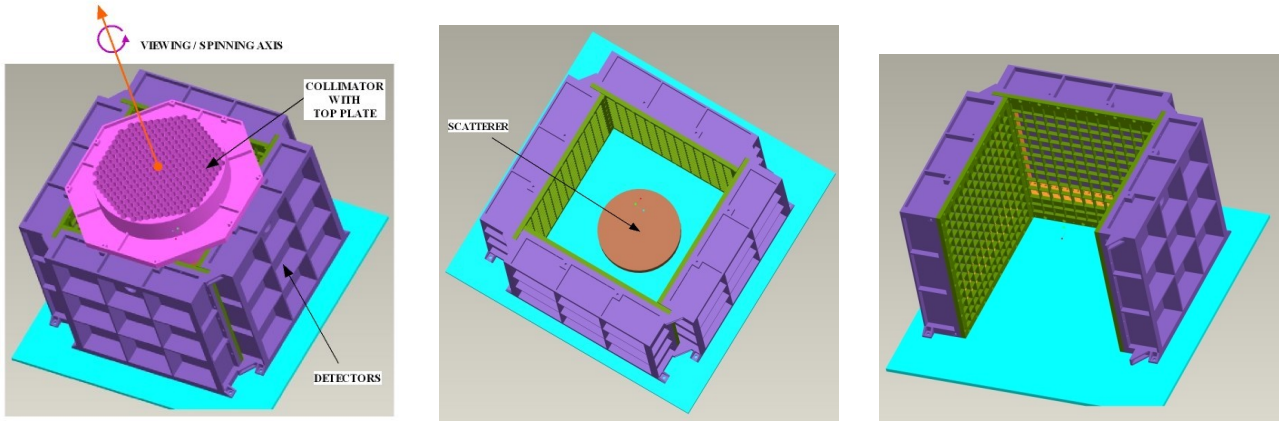


(a) (b) (c)

Figure 4.2: Design and Components of POLIX. Figure (a) shows the complete design with collimator on top and the rotation axis of instrument. Figure (b) shows the scatterer position. Figure (c) gives a view with one detector removed. It clearly shows the aluminium top-plate and the active volume (Yellow region behind the top-plate.). Image source : Polix Instrument Report, RRI, 2015.

The expected energy range is 5-30 keV with efficiency about 1 to 6 %. The large loss of efficiency is due to the forward and backward scattered photons, and due to the photons

absorbed in the scatterer and aluminium top-plate. However, as discussed in Sec. 4.4 the simulation results shows that the energy range can be stretched up-to 50 keV with efficiency still being about 1 to 6 %. All the four detectors and the collimator are ready. Currently, the work to integrate back-end electronics into small boards that can be fit at the back of the detector is in progress. Size, geometry and material of the scatterer is not fixed yet. Simulations carried out in section 4.4 gives more insight into scatterer position and material. Mostly low-z material Beryllium or Lithium or combination of both will be used as the scatterer. Detailed discussion and results carried out with various geometries for scatterer and detector can be found in Reference [11]. Although from the discussions in the paper it is clear that a cylindrical geometry for proportional counter is preferred because of its uniformity, the square geometry is selected due to the mechanical issues faced in keeping the cylindrical gas volume sealed.

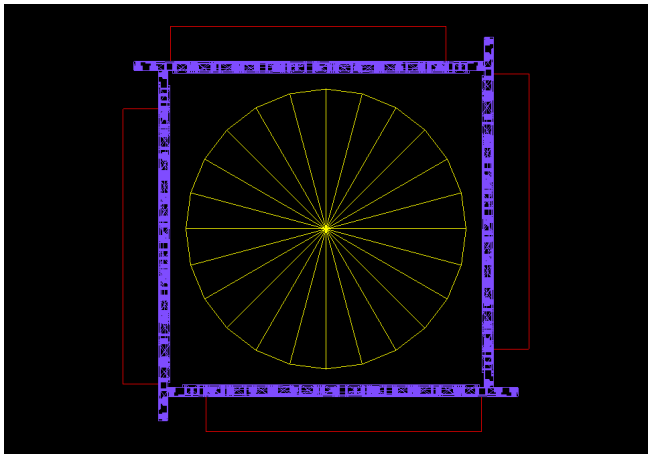

Figure 4.3: Top view of visualisation of instrument created with Geant4 showing the offset of active volume w.r.t. the centre of the instrument. Red boxes represent the active volume, yellow disk is the scatterer, while blue slab is the aluminium top plate used to support against the gas pressure inside the detectors.

## 4.3 Calibration of POLIX Detectors

As discussed in previous section, position sensitive proportional counters are used to determine the position of scattered photon. By determining this position we can find the angular distribution of photons, which intern can give us the modulation factor. As each proportional counter has twelve wires, detail calibration is needed to determine the position of incident X-rays. We are limited in accuracy in one axis (lets call it x-axis) as there are only 12 wires but on vertical axis we can achieve position resolution of about 1 cm. Analysis of data over a wide energy range, taken by an earlier calibration method, indicated energy dependence of the calibration parameters and a new calibration method was developed, in which the energy dependence is incorporated. Both the methods, along with the issue are described in the next two sections.

### 4.3.1 Initial Calibration Method

This calibration method was carried out earlier at two X-ray energies, with two radioactive X-ray sources. In this method, X-rays were shined at particular position on wire using a metal

plate with holes at pre-calibrated locations (Fig. 4.4). Each wire is named as X1 to X6 while each vertical position is named as Y1 to Y3 starting from bottom. Cd-109 (∼23 keV) and Fe-55 (∼6 keV) were used as X-ray sources. The idea here is to measure ratio value given by equation 2–8 given in Sec. 2.3 for known physical position. Since the wire has uniform resistance per unit length, by measuring ratio value for 2 or more positions we can interpolate and extrapolate ratio vs. position dependence. Hence, by measuring ratio value of incident photon we can determine its interaction position on the wire.

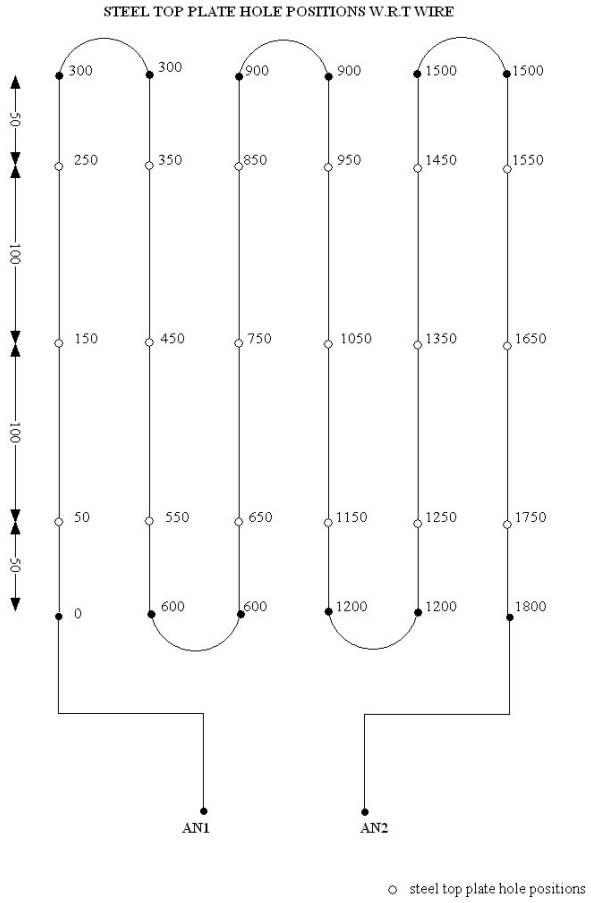


Figure 4.4: Calibration configuration for CH1 : Empty circles indicate hole positions.

#### 4.3.1.1 Data Analysis and Results

Data generated by this method was analysed in this project. To determine the ratio value corresponding to positions marked on the steel plate, ratio histogram was plotted for each wire. One such sample histogram, corresponding to wire 1 positions and energy 6 keV (Fe-55 line), is given in Figure 4.5. By fitting a Gaussian to such histogram we can find the mean ratio value for a particular position. Although, the energies of sources were 23 and 6 keV, additional energies were also observed due to the fluorescence from copper wire (∼8 keV) and Argon gas (∼3 keV, used as quenched gas along with methane in small amount). Figure 4.6 shows spectra for both the sources. Ratio histogram for these energies were also plotted. Ratio values for each position on given wire were then fitted with a straight line for get slope and intercept values for each wires which can be used to interpolate or extrapolate any arbitrary ratio value. Figure 4.7 shows such fit for one wire.

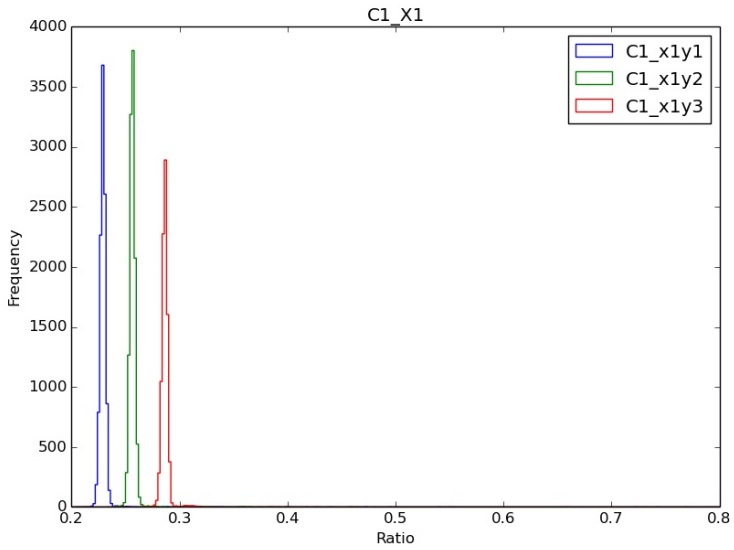


Figure 4.5: Ratio histogram for first wire at 6 keV : Blue = 50 mm; Green = 150 mm; Red = 250 mm. CH1 corresponds to output channel no. 1

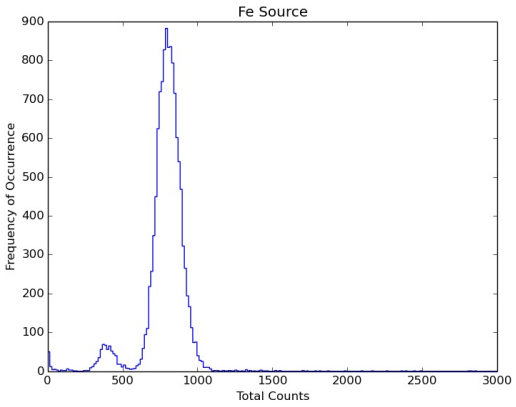


(a) Fe Source Spectrum. Small peak corresponds to 3 keV while big peak corresponds to 6 keV.

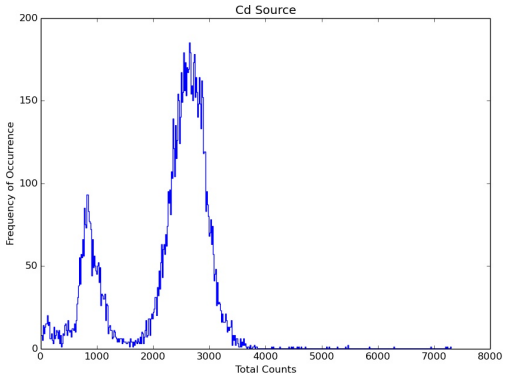


(b) Cd Source Spectrum. Small peak corresponds to 8 keV while big peak corresponds to 23 keV.

Figure 4.6: Spectrum for Cd and Fe Source

One interesting observation was made with the 8 keV photons. Whenever a ratio histogram is plotted for only one particular position, a side peak would appear at the ratio value of adjacent position on other wire. This is due the fact that fluorescence photons from wire are emitted isotropically. Although, most of the photons are absorbed at the same location, some photons escape and produce a signal on adjacent location on next wire and/or previous wire. Figure 4.8 clearly shows this observation.

#### 4.3.1.2 Energy Dependence of Ratio Values

Although the method yielded good results for individual energies, it showed some discrepancy when position vs ratio plots were compared for all the four energies. Figure 4.9 shows this issue. For same position value, ratio value varies as energy is changed. This means that ratio value has an energy dependence. This is not a trivial thing to expect as ratio value is nothing but

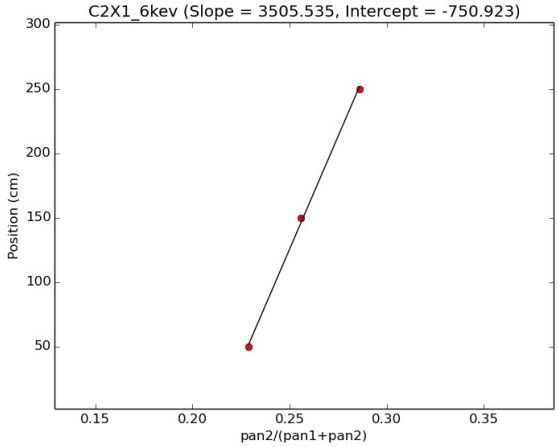


Figure 4.7: Position vs. Ratio plot for Wire 1 in output channel 2.

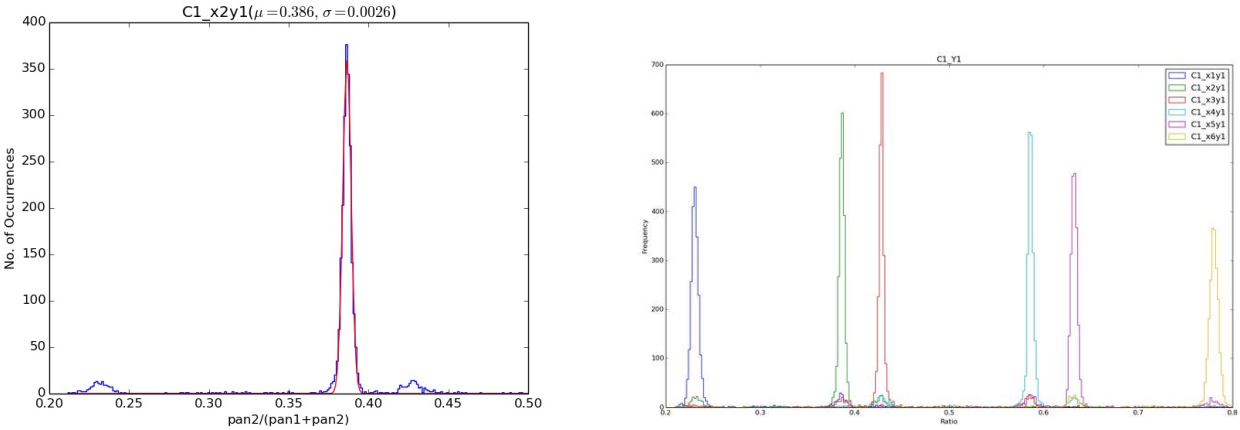


(a) X2Y1 position

(b) All Y1 positions

Figure 4.8: (a) X1Y1 : The left peak corresponds to X2Y1 and right peak corresponds to X3Y1, (b) Plot of all Y1 peaks, it clearly shows that all small peak fall under main peaks on adjacent wires.

fraction of charge collected at one end compared to the total charge. Although, total charge depends on energy, the fraction should not differ as the resistance of a wire is uniform. Also, statistical fluctuation were ruled out as Fig. 4.9 clearly shows some trend between energy values and the corresponding position vs. ratio plot. Low energy shows less ratio value compared to high energy for initial positions but the trend is reversed for end positions. To investigate further and to quantify this energy dependence some further analysis was done.

#### 4.3.1.3 Attempts to Quantify the Energy Dependence

After establishing the energy dependence of ratio values, we tried to quantify this dependence as calibration for all the energies is not possible. First we plotted slope values for each wire against energy (Fig 4.10) to find any functional dependence. As it is clear from the figure, we couldn't find any dependence which can be modelled accurately. Hence we shifted our attention to the end resistance i.e. the resistance between the two ends of consecutive wires. This is because if the end resistance is dependent on energy the ratio value could depend on energy. Hence by modelling end resistance we can correct for ratio value. To analyse this

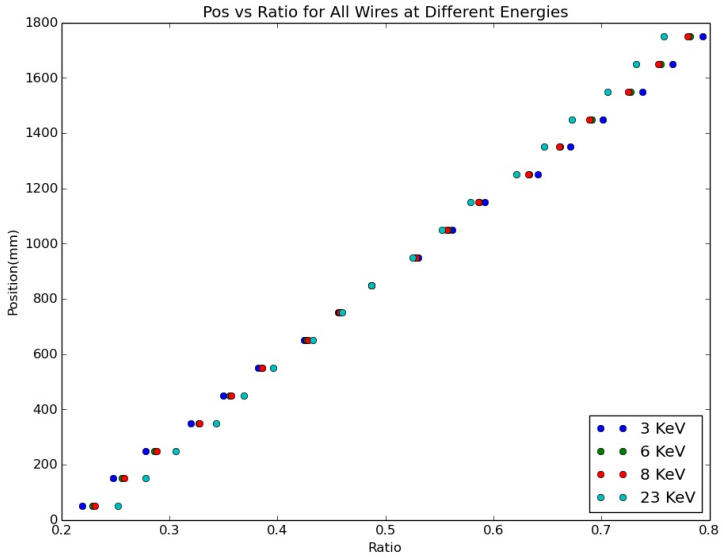


Figure 4.9: Position vs. Ratio plot for all energies and all 6 wires.

we converted the resistance to the equivalent distance value and observed the behaviour with energy. The equivalent distance was calculated by the following formulae,

$$Equivalent\ Dist. = (R_{1,i} - R_{2,i-1})m_{i-1} \tag{4–9}$$

where, $i \in$ wire number. Figure 4.11 shows the plot of equivalent distance against gap no for different energies. It is clear from the plot that again there is no functional dependence and hence even this attempt to establish the energy dependence of ratios was not successful. Due to these findings we were forced to devise a new method to calibrate the ratio values against the physical position; which takes into account the energy dependence as well.

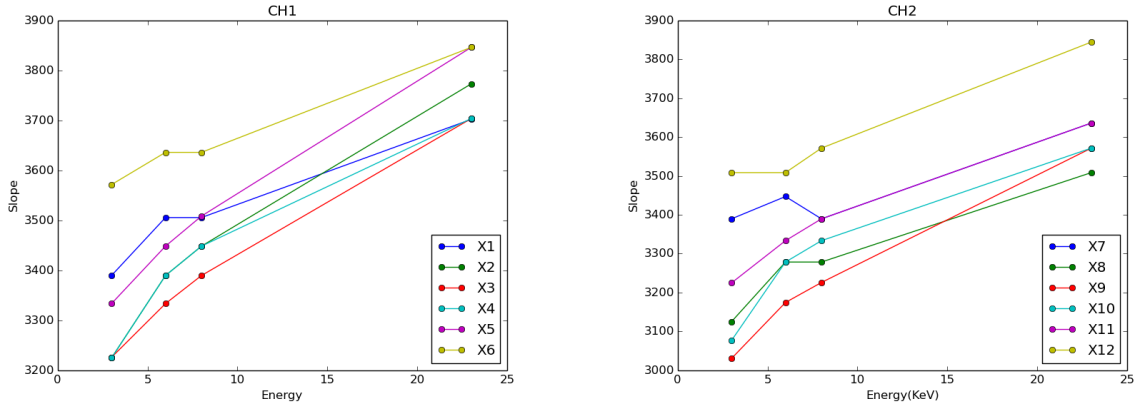


(a) CH1 (b) CH2

Figure 4.10: Slope (mm/unit ratio) vs. Energy plot for output CH1 and CH2

### 4.3.2 New Calibration Method

As the previous calibration method discussed above was having issues which could not be resolved easily, we adopted a different approach. We used the fact that if we bin the energy

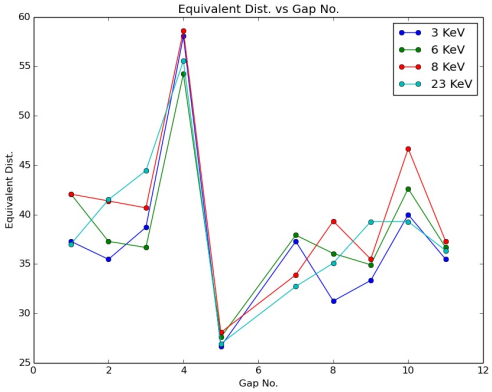


Figure 4.11: Equivalent distance for different energies and wire joints.

range such that the variation of ratio value for given position within the bin size is comparable to the spatial resolution achievable with these detectors, we can treat energy bin as one energy and define parameters for several such bins covering the entire range. Binning energy is equivalent to binning channel no. of pulse height spectra. The idea here is to get ratio distribution for all the wires for given bin and then find ratio bounds for each wire for that particular bin. Physical position of a ratio value belonging to that channel bin can then be found by interpolating ratio bounds with a straight line for individual wire.

To check this method, new data was needed, hence we carried out following experiment. This experiment was carried out by me in collaboration with X-ray lab members of Raman Research Institute during months of August and September 2015. We shined X-rays from Cd-109 source on detector for total of 240 minutes with data collected every 30 minutes due to the output file size restrictions. Here, instead of shining X-rays via hole we shined them on all six wires (only one output channel was used) as we were looking for ratio value distribution for all wires. The Cd source was kept about a meter apart from the detector to get reasonable uniform exposure. Figure 4.12 show the experimental setup.


Figure 4.12: Experimental setup for the new method. The small disk on the stand is the Cd source. Behind each vertical array of squares, anode wire runs through the centre. As only six wires were used, the source has offset compared to the centre of detector.

#### 4.3.2.1 Results and Analysis

At the time of this experiment, the detector had poor energy resolution because of contamination by water vapours. The active volume is sealed with a Mylar window at the front (behind the square ribs). Although Xenon can't penetrate through Mylar, water vapour can. Since the detector was not kept in sealed containers, contamination by water vapour was observed. As explained in Sec. 2.2.4, the resolution highly depends on fill gas and hence any impurity damages the resolution. Due to this we observed a broadband spectrum for Cd source, although Cd emits only at 23 keV. Figure 4.13 shows the observed spectrum.

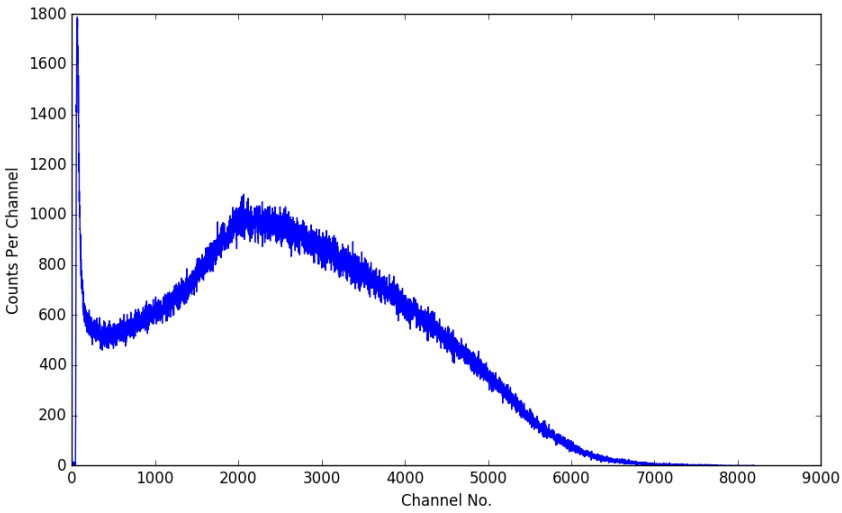


Figure 4.13: Cd spectrum observed as broadband spectrum due to poor resolution. Compare this with Cd spectra shown in Fig. 4.6 when resolution was good.

However, this poor resolution was useful in this method as we need to bin channel no. into small bins and broadband spectrum means we can cover larger range. Entire channel range was divided into channel bins containing 100 channel each. For each bin, ratio histogram for all six wires was plotted. Figure 4.14 shows one such histogram for channel range 900 to 999. The large dips in the counts marks the end of the wire. While small dips are due to the aluminium top-plate seen in Fig. 4.12. By manually setting a common cut-off value for counts which marks the end of all wires, ratio bounds of all six wires were obtained for each channel bin. These 14 numbers, two channel bounds and 12 ratio bounds, 2 for each wire, were written into a output file for each bin. This file is then a calibration file for the detector. Now, if we want to determine a position of any interaction, first we should find the channel bin to which the event belongs and then find the wire by comparing the ratio value against the ratio bounds. Once we determine the wire, we can find the physical position by interpolating the ratio bounds and by applying the interpolation relation to the ratio value of the given event. For this particular dataset, channels ranging from 500 to 5200 were considered as other values of channel no. had limited statistics. The great advantage of this method is that it can do self calibration for a data set with broadband spectrum. As this is the case for any background spectrum or most of the astronomical sources, the instrument can be calibrated simultaneously as it acquires science data.

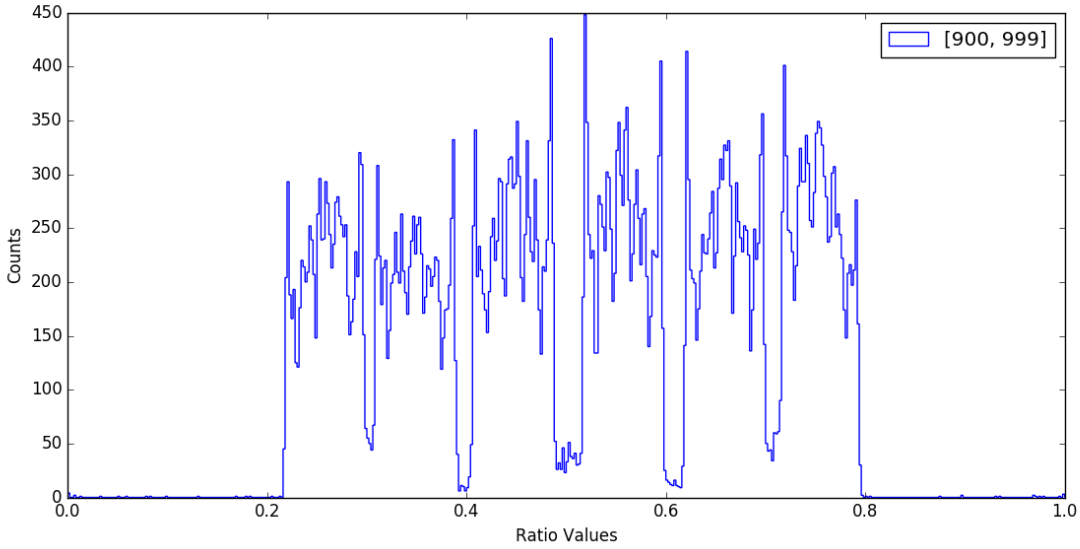


Figure 4.14: Ratio histogram for all six wires for channel range 900 to 999.

#### 4.3.2.2 Pipeline For Future Calibration

As this calibration method will be used to do the calibration in future, I wrote a small pipeline to calibrate the data. The codes are written in python. It consists of three major programs out of which two require inputs from user. The first program is to generate a output file with list of the channel bin for which the calibration is to be done. This program asks for user inputs such as channel bounds and bin width. The second program executes the processes describes in previous section. This program loops over 4 detectors and 2 output channels for each detector. When executed it asks for detector and output channel for which the calibration has to be done. Then it takes output file of previous program and data files from detector as input and for each channel bin defined the input file and plots a histogram similar to Figure 4.14. User has to manually select the cut-off and enter the value. Output of this program is a file with ratio bounds for each wire written in front of the channel bounds. Total 8 such files will be created. The third program doesn't require any user input. It takes files created by second program and data files as input. For each event in data file, it calculates the total channel no and ratio and finds the appropriate wire to which the event belongs and by interpolating ratio bounds it finds the physical position of the event. This position is appended in front of each event in the data file and file is saved as new output file. To check whether the this method and pipeline is working, a count map for acquired Cd-109 data was created. Figure 4.15 shows the map for 6 wires. The dips in counts are because of the Aluminium frame ribs. About 13.6 % photons are lost as they do not lie between any ratio range. However, this no. can be reduced by reducing channel bin width. Currently bin width of 100 channels is used.

This completes our discussion about the establishing calibration method for detectors. In next section, I will discuss the results we obtained from simulations I carried out in Geant4 by implementing actual geometry.

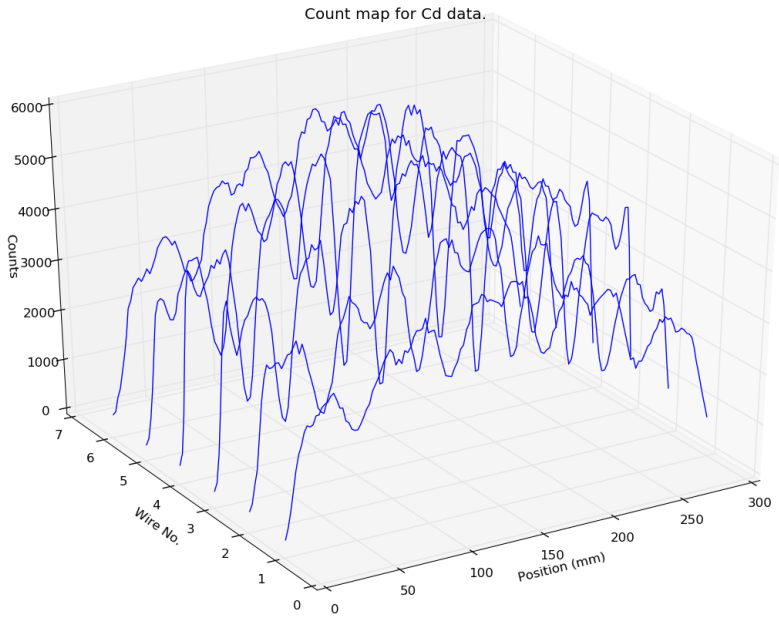


Figure 4.15: Count map for Cd data for six wires

## 4.4 Simulations of POLIX With Geant4

Another part of my work with the X-ray polarimeter involved carrying out simulations with actual detector geometry but varying scatterer material, position, polarisation of incident photons and spectral index of incident photon distribution. Simulations were carried out in Geant4 - a simulation toolkit developed by CERN for particle matter interactions. Introduction to Geant4 is given in Appendix A. However, in next section, I will give a brief insight about algorithm and method in which the simulations were carried out.

### 4.4.1 Implementation in Geant4

Geometry of the detector was constructed using the G4VUserDetectorConstruction class in Geant4. The top-plate geometry was directly imported from AutoCAD, a program used to design and construct mechanical structures. To import the top-plate geometry from AutoCAD output to Geant4, external library developed by Christopher Poole[1] was used. Active volume and scatterer was build using standard Geant4 shapes G4Box and G4Tubes. The gas used to fill was Xenon at 800 torr pressure.

To simulate physics, predefined physics list, G4EmLivermorePolarizedPhysics , which simulates polarised processes involving light was used. G4GeneralParticleSource was used to create primary particles, in this case the are incident photons. Photon distribution was either mono-energy Gaussian or power law depending upon the simulation type discussed in next section. Also, for one particular case, polarisation of incident photons was also varied. The no. of total photons was a varying no. depending on the simulation type.

[1] https://github.com/christopherpoole/CADMesh

When simulation is started, Geant tracks each primary particle (in this case a X-ray photon) and secondary particles (in this case mostly electrons created by the interaction) until they are destroyed by absorption or leave the simulation 'world volume'. Entire instrument volume must be contained inside the world volume. By using G4VUserSteppingAction class the user can track any particle (with all its physical parameters) as it progresses through the detector volume or world volume at each 'step'. A step is analogue of a time snapshot of particle. As we are only interested in no. photons absorbed in active volume, information about particle was extracted only when a step records an photoelectric interaction in the active volume. The parameters which were extracted for such events were, event no., which is between 0 to total no. photons for which simulation is carried out and x,y,z coordinates of the photoelectric interaction. All this data was written into a file at the end of the Geant4 run. Multi-threading mode, mode where Geant uses all the available CPU cores for processing, was used to reduce the simulation time. This data was then analysed using python codes depending upon the type of analysis.

### 4.4.2 Simulation Types

Actual detector geometry was simulated to carry out the simulation. The simulated geometry consisted of 4 square Xenon gas boxes on a side of a square(representing the four proportional counter volumes) with a scatterer in the middle. The boxes were build behind the Aluminium top-plates (to simulate the shadow effect it will create in case of an actual detector) and a Mylar window (used in actual detectors to seal Xenon gas but to allow X-rays). The scatterer shape was fixed as a disc with radius of 18 cm. Figure 4.3 shows the geometrical construction of instrument in Geant4 (top view). Three types of simulations were carried out with Geant. First simulation involved optimising scatterer material. This was carried out for discrete energies in steps of 5 keV in range 5 to 50 keV. For each energy, simulation was carried out for 10 million incident photons keeping the polarisation fixed in x-direction. Material used were Beryllium, Lithium and combination of Lithium and Beryllium with Lithium on top. The shape of the scatterer was a disc with radius 18 cm. To get sufficient scattering coefficient, a material surface density of 12 - 14 $cm^2/g$ is needed. Keeping this no. as constant, height of the disc was varied according to the material density.

Next simulation was done using the results of the previous simulation. For the reasons discussed in next section, optimal configuration for scatterer was selected as Li-Be disc with total scattering being equal to 12.9 $cm^2/g$. With this fact established, power law distribution for incident photons was used with the index changed in step of 0.5 between -0.5 to -3.5 for each run. Minimum value of energy was 5 keV and maximum value of energy wad 50 keV. Total no. of photons were again 10 million which would be distributed according to index. In this case the spectra was continuous unlike the previous one. Also, for each index, position of the scatterer along the z-axis was varied. Total six positions were covered, with first position being when the boundary of Li-Be interface is at the centre of the entire instrument and last being when the bottom of the Be slab touches the bottom of the instrument. Dependence of efficiency on index and height was studied.

Third and the last simulation was carried out to get the modulation factor for this detector configuration and Li-Be scatterer placed midway between bottom and centre of the detector. For this, spectral index of power law was kept as constant at -2. Min. and max. energy values were same as above. Now, the polarisation of incident photon was varied between each run from 0 to 180 degrees in steps of 1 degree. Due to file size and simulation time constraints, total no. of photons were reduced to 50 million. However, as we shall see in next section, results from each run were co-added, reducing total no. didn't affect the statistics.

### 4.4.3 Results and Analysis

For first simulation, no. counts in each detector for the discrete energies was converted to counts one would observe if the spectra was a power law. This was done by multiplying the existing value with $E^{-\alpha}$ where $\alpha$ is spectral index and $E$ is corresponding energy. This was done for $\alpha = 1, 2, 3$. The efficiency was then calculated by dividing total no. photons in each run which is 10 million. This efficiency (not corrected for power law) against energy for all the three materials (Be, Li and Li-Be) and for different position is shown in Figure 4.16. For Li-Be Mid-way, the efficiency corrected for power law spectrum is shown in Figure 4.17. From

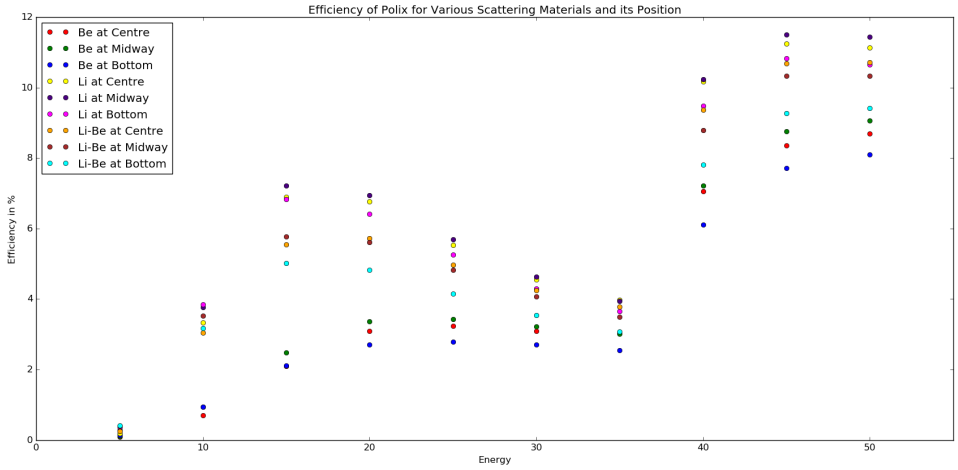


Figure 4.16: Efficiency of POLIX for all materials kept at different heights.

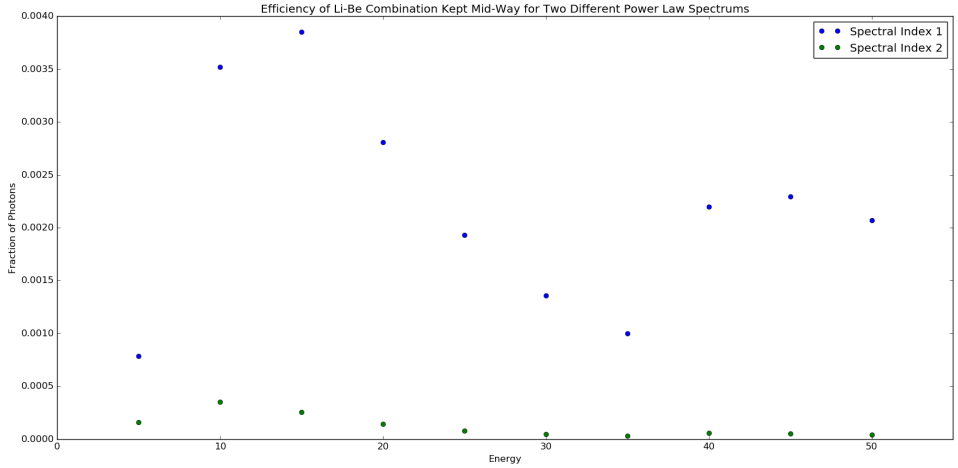


Figure 4.17: Efficiency of POLIX for Li-Be combination kept at Mid-way for different spectral indices.

plots it is clear that Li scatterer gives the best efficiency among three choices, however, to keep the required scattering efficiency, if choose only Li as scatterer the height of the disc becomes 21 cm. In case of Lithium, it being a toxic material, handling such huge scattering volume is not possible. Hence, the next best choice, the Li-Be combination was selected for future simulations. In this case the Li disc height reduces to 11.5 cm while Be disc height is 3.5 cm.

Aim of the second simulation was to study the variation of detector efficiency as function of height and spectral index of incident photons. The data obtained from this was used to plot a surface plot with X and Y axis as spectral index and scatterer position centre while Z axis as detector efficiency. Figure 4.18 shows the plot in two different angles. The height is measured from centre of the detector with zero being the configuration when Li-Be boundary plane is at the centre while 5 being the configuration when Be disc bottom plane is touching the bottom of the detector. 1, 2, 3,4 corresponds to the position when Li-Be boundary plane is at $1/5^{th}, 2/5^{th}, 3/5^{th}, 4/5^{th}$ of the distance between centre and bottom position, respectively.

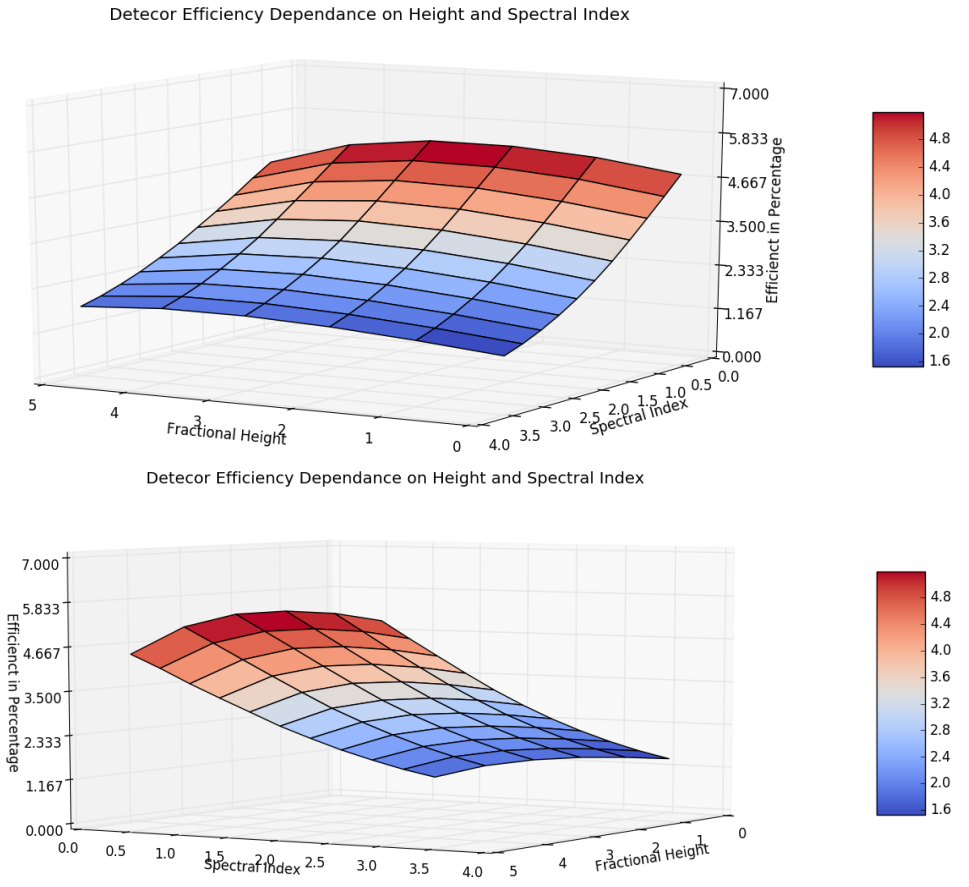


Figure 4.18: Dependence of detector efficiency on scatterer position and photon spectral index

The conclusion from this exercise was that for lower spectral index (hard X-ray sources), to achieve maximum efficiency, it is better to keep the scatterer mid way between centre and bottom. While for higher spectral index (soft X-ray sources) maximum efficiency can be obtained by keeping scatterer close to the bottom. This is expected as hard spectra implies more photons in higher energy band hence amount of forward scattering is more and hence by keeping the scatterer at mid-way we can increase the probability of forward scattered photon to be detected

thus increasing the efficiency. While for soft X-rays most of the photons have low energy and hence are mostly absorbed or back scattered. Hence, by keeping the detector close to bottom, we can increase the efficiency by increasing the probability of back scattered photons to be detected in active volume.

One separate run with spectral index 2 and scatterer at the bottom was done to show the distribution of all the photons in the instrument. Also, photons escaped from the instrument was recorded by placing a 3 mm lead shell enclosure. The run was only for 500 thousand photons to limit the data and plotting size. The distribution is shown in Figure 4.19. The photon incident direction is -ve z. The data for above plots is tabulated in table 4.1. Notice that majority of the photons are absorbed in the scatterer and many are absorbed in the Aluminium top-plate. Absorption in these volumes is major reason for low efficiency. The

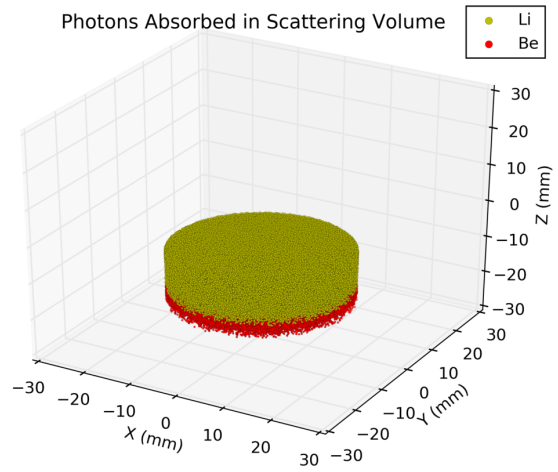


(a) Photons absorbed in scatterer

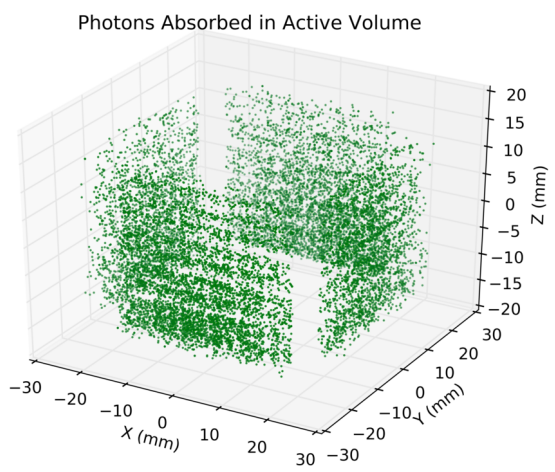


(b) Photons absorbed in all detectors

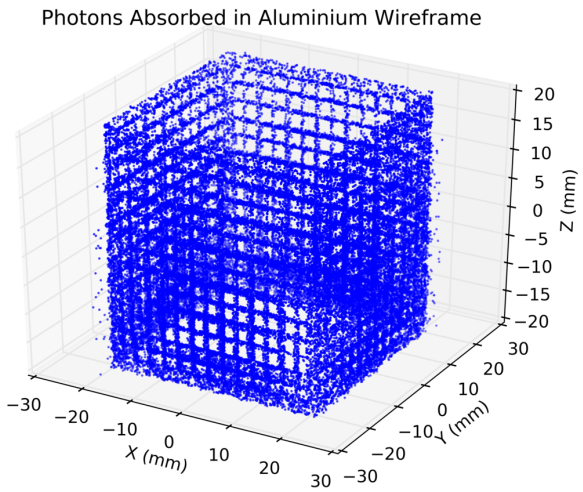


(c) Photons absorbed in Aluminium top-plate.

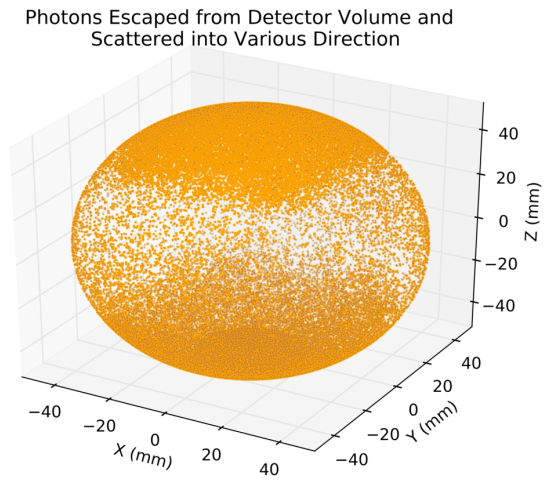


(d) Photons absorbed in Lead shell enclosure

Figure 4.19: Distribution of photon in various components of the instrument.

shadow due to the top-plate can be clearly seen in the Fig. 4.19b. Also, in the lead shell volume we can clearly see that the majority of the photons are either backscattered or forward scattered.

| Volume | No. Photons Abs. | Percentage |
|---|---|---|
| Beryllium | 60006 | 12.01 |
| Lithium | 289317 | 57.86 |
| Top-plate | 66005 | 13.2 |
| Detectors | 13950 | 2.79 |
| Lead | 70722 | 14.14 |

Table 4.1: Data for Fig. 4.19. The percentage is relative to total no. of incident photons, which is 500,000.

The third and final simulation was done to determine the modulation factor for this geometry and scattering material. The equation 4–5 tells us that the scattered photons are distributed in a donut with axis along the direction of electric field. Hence, if incident photons are polarised in one direction and say the instrument x-axis is aligned with the direction of polarisation, the maximum no. of scattered photons will be detected on the detectors which are parallel to the instrument x-axis and less will be detected on the detectors perpendicular to the direction of polarisation, i.e. detectors parallel to the y-axis of the instrument. Now if we change the polarisation by 90 degrees, result will be vice versa. This is clearly visible in Fig. 4.20. The figure represents xy plane of instrument with z-axis suppressed. The left plot is distribution of photons when the polarisation is in x-direction, hence more photons in top and bottom detectors compared to left and right detectors. While in the left plot the polarisation is changed by 90 degrees, hence the resulting distribution is reversed.

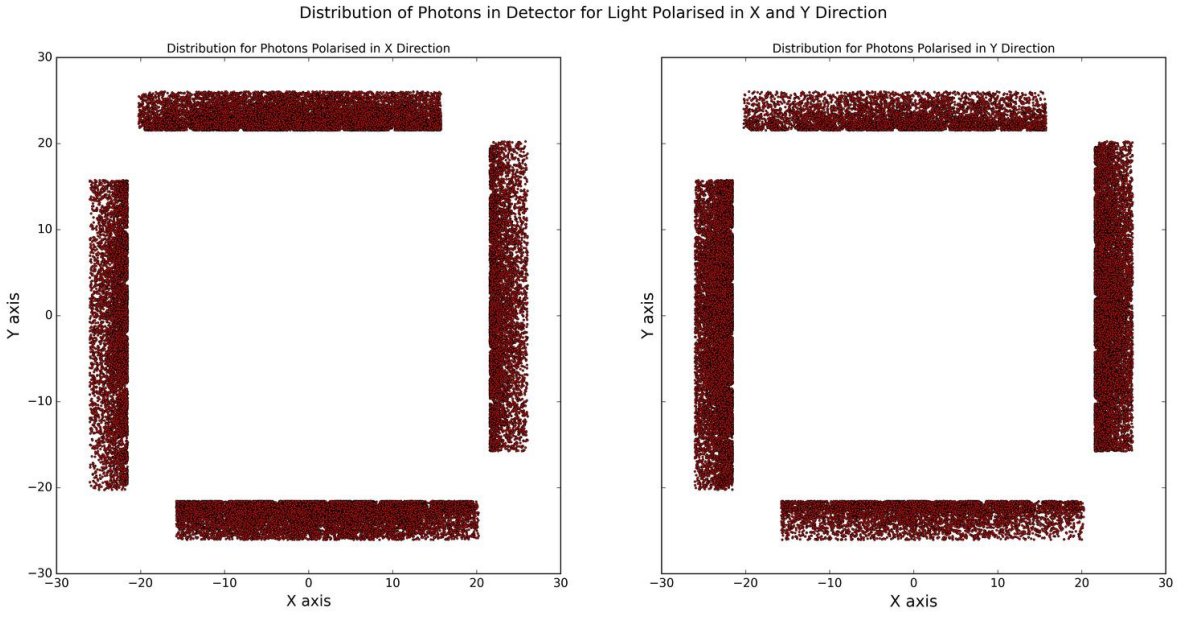


Figure 4.20: Distribution of photons in detector for two different polarisations.

In this simulation exercise, the polarisation angle was changed from 0 to 180 degrees. This is equivalent to rotating instrument by keeping the polarisation fixed. This will be the case in real observations as, while observing one source, the entire instrument will be rotating. As polarisation angle changes, it will produce different distribution of photon, phase shifted by constant angle. The distribution, also called as modulation pattern, will have period $\pi$ as polarisation angle is symmetric between 0 to 180. Although the simulation allows us to predict exact location of photon interaction in detector volume, in practice we are limited by no. of wires in one detector (in case of POLIX 12) as we can only tell on which wire the photon is detected. Hence, the entire detector volume was divided into twelve 3 cm long vertical cells. The assumption was the anode wire runs through the centre of the cell and any photon detected within cell volume is registered on corresponding anode wire. By this way the all four detectors were divided into 48 wires. Now, each wire is an individual polarimeter. Because as the polarisation vector rotates the modulation pattern can be observed in each wire. The pattern will have $cos(2\phi)$ dependence discussed in section 4.2.1. For successive wires, this pattern will be shifted in phase which is equal to the angular separation between successive wires. Hence, if we co-add these wire by fixing one wire and correcting for phase of all the other wires we can obtain one single modulation curve for entire instrument and can calculate modulation factor by equation 4–8.

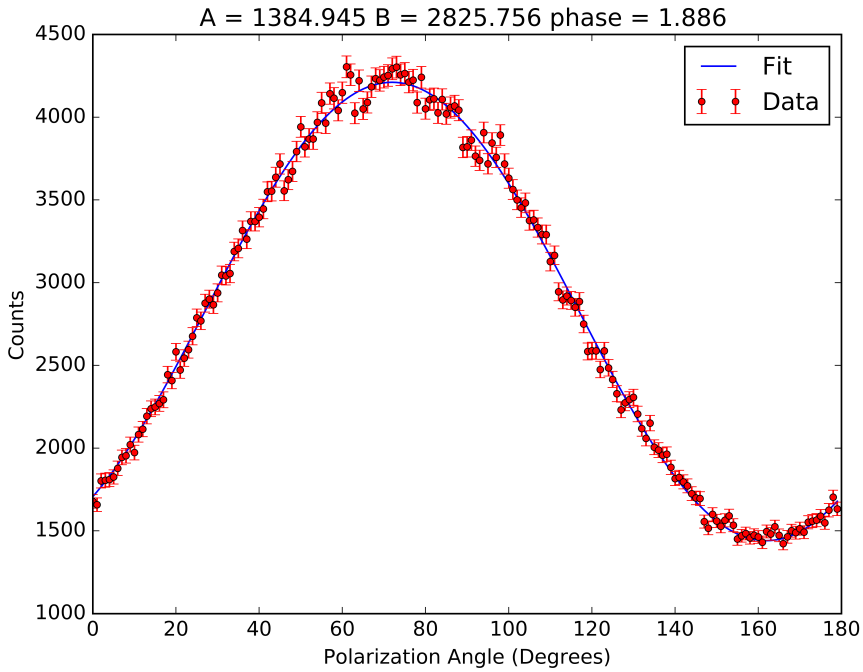


Figure 4.21: Modulation curve for single wire.

To get phase for each wire, modulation curve was plotted by counting no. of photons detected within cell corresponding to that wire for each polarisation angle and plotting counts against the angle. The plot was fitted with equation,

$$C(\phi) = Acos(2(\phi + phase)) + B \tag{4–10}$$

Phase for each wire was recorded. Figure 4.21 shows modulation curve, both data and model, for one wire. Although the period is 180, phase was recorded between -180 to +180 so that all the 48 wires can be brought to one location. The wire with maximum A value was selected as a reference and all the other wires were phase corrected. After phase correction, the counts for each angle were added to create a final modulation. The curve was again fitted using above equation and modulation factor with value equal to 0.444 was obtained. By this method, the statistics improve significantly minimizing the error in determining the modulation factor. The final modulation factor is shown in figure 4.22. Error bars aren't shown here as the point size is more than the error on each point.

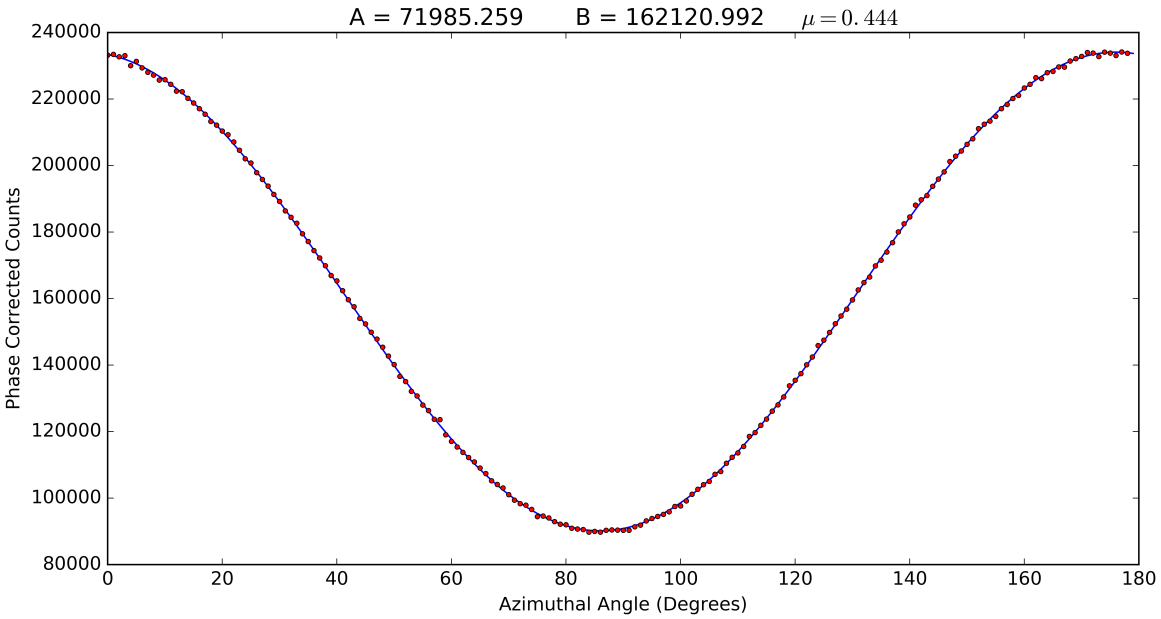


Figure 4.22: Final modulation curve for instrument

With this value for modulation factor, approximate calculation was done to get MDP estimates for crab like sources. To do this, background count rate from LAXPC data was taken and was scaled down according to the POLIX area and the efficiency which was obtained in first simulation (for Li-Be at midway). To get source count, normalisation of Crab at 1 keV (9 counts/sec) was used. By calculating area under the curve defined by equation 4–11, approximate count rate of Crab which will be observed by POLIX was calculated.

$$count\ rate(/keV/sec) = ANE^{-\gamma}f(E) \tag{4–11}$$

where,

$A$ = Area of active volume for POLIX = 650 $cm^2$

$N$ = Normalisation $\approx$ 9 counts/sec/$cm^2$ at 1 keV for Crab

$E$ = Energy of photon (keV)

$\gamma$ = Spectral index $\approx$ 2 for Crab

$f(E)$ = Efficiency dependence on energy

This gives value for both background and signal count rate around 32 counts per second. By assuming we demand 3-sigma confidence level, MDP value was plotted against different intensities (in terms of Crab unit) for 3 different exposure times, 30000 sec (approximately about a day's observation), 100000 sec and 300000 sec. The plot is shown in Figure 4.23. The plot shows MDP dependence of 5 different sources which would be observable by POLIX. From figure it is clear that for a source of given intensity, MDP decreases as exposure increases. Also, it shows that as intensity decreases MDP is highly dependent on the exposure time. This clearly shows the "photon hungry" nature of X-ray polarisation measurements.

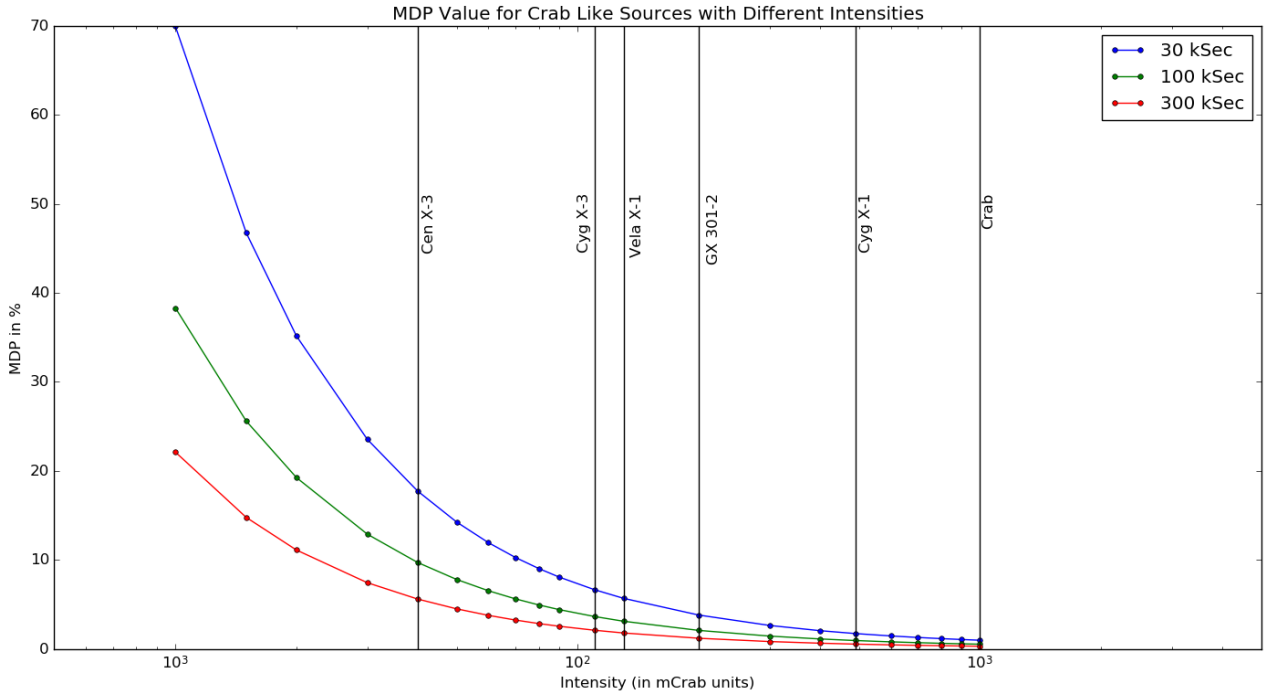


Figure 4.23: Minimum Detectable Polarisation dependence on source intensity and exposure time for POLIX

This marks the end of the discussion related to simulation of POLIX and the chapter as a whole. The code written for simulation is being documented for future use. Simulations such as optimisation of scattering geometry can be carried out in future by using this code. Based on modulation factor, optimal geometry can be selected. We expect some pioneering science results from the polarimetry mission and it will certainly be a benchmark for the future missions.

# Appendix A

# Appendix A

## A.1 Introduction to Geant4

To quote Geant4 official website[1], "Geant4 is a toolkit for the simulation of the passage of particles through matter". It is used in many areas such as high energy and nuclear physics, space physics and medical sciences. The toolkit provides large amount of flexibility in carrying out simulation as the building blocks of the toolkit are defined at an abstract level. Geant4 covers almost all aspects of a simulation process, which include following major features,

- Detail Geometry construction and large material database.
- All particle definitions with detailed properties.
- Generation of primary particle with various spacial, spectral and angular distributions.
- Large list of predefined physical processes with option to create user defined process.
- Detail tracking of particles through matter and generation of secondary particles based on physical processes with option to write data at each step.
- Visualisation of detector and particle interaction.

The software is written in *C++*, hence reasonable knowledge of the language is needed to build any simulation. As it follows object oriented programming, knowledge about classes and their use is necessary. Although Windows version is available, usage on Linux is preferred as more features are supported (e.g multi-threading is not supported on Windows but it is supported on other platforms). Block diagram in fig. A.1 shows how geant runs a particular simulation. A *Run* in Geant4 is an equivalent of carrying out an experimental run with no change in detector configuration. A run consists of *Events*, usually equal to the no. of particles for which the simulation is to be carried out. For each event, all the particles are tracked until they are destroyed or leave the "world" volume. The particle information at each instance is stored in a *Track*. This information is updated in delta of *Step*. All these are defined as classes and any information stored in each object can be extracted by properly instantiating the object of these classes. When `main()` function is called, it instantiates G4RunManager class

[1] http://geant4.cern.ch/

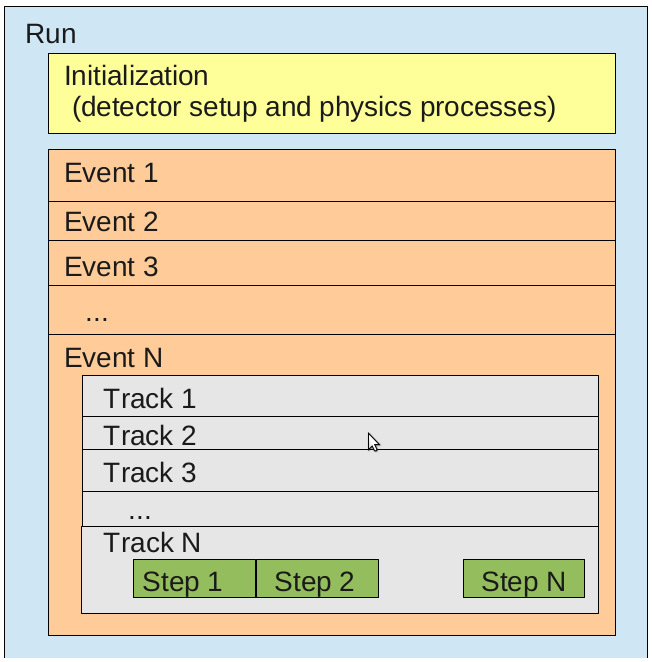


Figure A.1: Block diagram of Geant4 kernel. Image adopted from Reference [5]

which manages the geant4 runs. When a run is initialised, geometry and physics processes are initialized and the simulation is in "beamOn" state (analogues to staring particle beam in real world). Geant then simulates physics and tracks particles in a way mentioned above until all the events in a given run are processed. Building a simulation is not a trivial job, however it can be summarised in following steps,

- Geant4 developers have defined abstract classes, user has to derive all necessary classes from these and defined his own methods inside it. Some of them are mandatory.
- These classes are called and instantiated in `main()` function. This program just manages overall run, all the definitions of geometry, physical processes, primary particle and tracking and storing necessary data has to be done in classes created in above step.
- User has to create mandatory classes ActionInitialisation class (which creates primary particles and sets other parameters), DetectorConstrunction class (where detector geometry is defined and is constructed when `main()` function is called and PhysicsList class (where physics which is t be simulated is defined). User can create additional classed such as SteppingAction class (by which he/she can extract information at each step of simulation).
- User can optionally select to analyse the data with G4AnalysisManager classes, however one can always write output to a file and analyse is with external program.

Geant4 is a powerful tool for simulation as it provides such high level flexibility in carrying out simulations with very accurate results. It is very important in HEP simulations to test detectors as it not always possible to carry out test experiments in such high energy regimes. There are many tutorial available online for Geant4 and one can be comfortable with it with some efforts. It is definitely a handy tool for those who work in the area where HEP experiments are carried out.

# References


[1] Agostinelli, S., Allison, J., Amako, K. *et al.*. GEANT4 - a simulation toolkit. *Nuclear Instruments and Methods in Physics Research A*, 506:250–303, July 2003. doi:10.1016/S0168-9002(03)01368-8.

[2] Arnaud, K. A., Dorman, B. and Gordon, C. XSPEC - An X-Ray Spectral Fitting Package. https://heasarc.gsfc.nasa.gov/xanadu/xspec/manual/manual.html, July 2015.

[3] Bradt, H. *Astronomy Methods: A Physical Approach to Astronomical Observations*. Cambridge University Press, January 2004.

[4] George, I. M., Arnaud, K. A. and Ruamsuwan, L. The Calibration Requirements for Spectral Analysis. https://heasarc.gsfc.nasa.gov/docs/journal/calibration_rqmts2.html, 1992.

[5] Hrivnacova, I. Geant4 tutorial for ED MIPEGE(Session 1) - Kernal. https://ivana.home.cern.ch/ivana/ED-Geant4/presentations/I-3-kernel.pdf, May 2013. Presentation Slides.

[6] Kaaret, P. X-Ray Polarimetry. *ArXiv e-prints*, August 2014. 1408.5899.

[7] Knoll, G. F. *Radiation Detection and Measurement*. New York, NY: Wiley, 3rd edition, 2000.

[8] LAXPC Team. Calibration of LAXPC Detectors. Technical Report, TIFR - Mumbai, January 2013.

[9] Paul, B. Astrosat: Some Key Science Prospects. *International Journal of Modern Physics D*, 22:1341009, January 2013. doi:10.1142/S0218271813410095. 1307.5637.

[10] Seward, F. D. and Charles, P. A. *Exploring the X-ray Universe*. Cambridge University Press, August 2010.

[11] Vadawale, S. V., Paul, B., Pendharkar, J. *et al.*. Comparative study of different scattering geometries for the proposed Indian X-ray polarization measurement experiment using Geant4. *Nuclear Instruments and Methods in Physics Research A*, 618:182–189, June 2010. doi:10.1016/j.nima.2010.02.116. 1003.0519.

[12] Weisskopf, M. C., Silver, E. H., Kestenbaum, H. L. *et al.*. A precision measurement of the X-ray polarization of the Crab Nebula without pulsar contamination. *ApJL*, 220:L117–L121, March 1978. doi:10.1086/182648.